

Development of a Rapid Assessment Tool for Pile Capacity and Stability in Response to Scour Situations

Final Report
March 2018



IOWA STATE UNIVERSITY
Institute for Transportation

Sponsored by
Iowa Department of Transportation
(InTrans Project 16-564)
Federal Highway Administration

About the Bridge Engineering Center

The mission of the Bridge Engineering Center (BEC) is to conduct research on bridge technologies to help bridge designers/owners design, build, and maintain long-lasting bridges.

About the Institute for Transportation

The mission of the Institute for Transportation (InTrans) at Iowa State University is to develop and implement innovative methods, materials, and technologies for improving transportation efficiency, safety, reliability, and sustainability while improving the learning environment of students, faculty, and staff in transportation-related fields.

Disclaimer Notice

The contents of this report reflect the views of the authors, who are responsible for the facts and the accuracy of the information presented herein. The opinions, findings and conclusions expressed in this publication are those of the authors and not necessarily those of the sponsors.

The sponsors assume no liability for the contents or use of the information contained in this document. This report does not constitute a standard, specification, or regulation.

The sponsors do not endorse products or manufacturers. Trademarks or manufacturers' names appear in this report only because they are considered essential to the objective of the document.

Iowa State University Non-Discrimination Statement

Iowa State University does not discriminate on the basis of race, color, age, ethnicity, religion, national origin, pregnancy, sexual orientation, gender identity, genetic information, sex, marital status, disability, or status as a U.S. veteran. Inquiries regarding non-discrimination policies may be directed to Office of Equal Opportunity, 3410 Beardshear Hall, 515 Morrill Road, Ames, Iowa 50011, Tel. 515-294-7612, Hotline: 515-294-1222, email eooffice@iastate.edu.

Iowa Department of Transportation Statements

Federal and state laws prohibit employment and/or public accommodation discrimination on the basis of age, color, creed, disability, gender identity, national origin, pregnancy, race, religion, sex, sexual orientation or veteran's status. If you believe you have been discriminated against, please contact the Iowa Civil Rights Commission at 800-457-4416 or Iowa Department of Transportation's affirmative action officer. If you need accommodations because of a disability to access the Iowa Department of Transportation's services, contact the agency's affirmative action officer at 800-262-0003.

The preparation of this report was financed in part through funds provided by the Iowa Department of Transportation through its "Second Revised Agreement for the Management of Research Conducted by Iowa State University for the Iowa Department of Transportation" and its amendments.

The opinions, findings, and conclusions expressed in this publication are those of the authors and not necessarily those of the Iowa Department of Transportation or the U.S. Department of Transportation Federal Highway Administration.

Technical Report Documentation Page

1. Report No. InTrans Project 16-564	2. Government Accession No.	3. Recipient's Catalog No.	
4. Title Development of a Rapid Assessment Tool for Pile Capacity and Stability in Response to Scour Situations		5. Report Date March 2018	
		6. Performing Organization Code	
7. Author(s) Yaohua "Jimmy" Deng (orcid.org/0000-0003-0779-6112), Brent Phares (orcid.org/0000-0001-5894-4774), and Ping Lu (orcid.org/0000-0002-9427-2415)		8. Performing Organization Report No. InTrans Project 16-564	
9. Performing Organization Name and Address Bridge Engineering Center Iowa State University 2711 South Loop Drive, Suite 4700 Ames, IA 50010-8664		10. Work Unit No. (TRAIS)	
		11. Contract or Grant No.	
12. Sponsoring Organization Name and Address Iowa Department of Transportation 800 Lincoln Way Ames, Iowa 50010		13. Type of Report and Period Covered Final Report	
		14. Sponsoring Agency Code SPR RB29-015	
15. Supplementary Notes Visit www.intrans.iastate.edu for color pdfs of this and other research reports.			
16. Abstract <p>The Iowa Department of Transportation (DOT) rating engineer is sometimes asked by field personnel to make quick decisions regarding pile capacity and stability when scour is identified around bridge pile bents. A numerical evaluation program was developed and implemented to offer a user-friendly assessment tool that can be used to quickly evaluate pile strength.</p> <p>The numerical program consists of finite element (FE) models established for steel H-piles with or without concrete encasement with consideration of linear and non-linear buckling and behavior. The research team validated the FE models against capacities calculated based on the provisions outlined in the American Institute of Steel Construction (AISC) Steel Construction Manual.</p> <p>After validating the FE modeling techniques, the researchers performed parametric studies to understand the influence of concrete encasement on the pile buckling strength. The individually encased pile bents in the P10L standard with five H-pile sections (HP10×42, HP10×57, HP12×53, HP14×73, and HP14×89) were utilized for the parametric studies. These studies took into account different combinations of the unbraced pile lengths and concrete encasement lengths. The relationships between buckling strength of the steel H-piles with concrete encasements under concentric and eccentric loading conditions were derived from the results of the parametric studies.</p> <p>The stiffness contributions of concrete encasements are not taken into account using the AISC Steel Construction Manual and American Association of State Highway and Transportation Officials (AASHTO) load and resistance factor design (LRFD) specifications for estimating the buckling strength of steel H-piles. The pile assessment tool that the researchers developed to quickly calculate the buckling strength of steel H-piles with concrete encasements includes the relationships between the buckling strength of steel H-piles with concrete encasement lengths for five cross-sections and two loading conditions. For the user's convenience, the researchers developed a graphical user interface for the tool, which requires the input of four parameters: loading eccentricity, H-pile section type, unbraced pile length, and concrete encasement length. This pile assessment tool can be utilized to quickly calculate the pile capacity and to assist state rating engineers in making rapid decisions regarding pile capacity.</p>			
7. Key Words concrete encasements—FE models—H-piles—pile bents—pile buckling—scour—steel pile assessment tool		18. Distribution Statement No restrictions.	
19. Security Classification (of this report) Unclassified.	20. Security Classification (of this page) Unclassified.	21. No. of Pages 68	22. Price NA

DEVELOPMENT OF A RAPID ASSESSMENT TOOL FOR PILE CAPACITY AND STABILITY IN RESPONSE TO SCOUR SITUATIONS

**Final Report
March 2018**

Principal Investigator

Brent Phares, Director
Bridge Engineering Center, Iowa State University

Authors

Yaohua “Jimmy” Deng, Brent M. Phares, and Ping Lu

Sponsored by

Iowa Department of Transportation and
Federal Highway Administration

Preparation of this report was financed in part
through funds provided by the Iowa Department of Transportation
through its Research Management Agreement
with the Institute for Transportation
(InTrans Project 16-564)

A report from

Bridge Engineering Center

Iowa State University

2711 South Loop Drive, Suite 4700

Ames, IA 50010-8664

Phone: 515-294-8103 / Fax: 515-294-0467

www.instrans.iastate.edu

TABLE OF CONTENTS

ACKNOWLEDGMENTS	ix
EXECUTIVE SUMMARY	xi
CHAPTER 1: INTRODUCTION	1
1.1 Background.....	1
1.2 Objective and Scope	1
1.3 Work Plan.....	1
Task 1 – Literature Review and Other Information Collection	1
Task 2 – Development of Assessment Tool	2
Task 3 – Documentation and Information Dissemination	2
CHAPTER 2: LITERATURE REVIEW	3
CHAPTER 3: NUMERICAL EVALUATION PROGRAM.....	4
3.1 Steel H-Piles without Concrete Encasement	4
3.1.1 Linear Elastic Buckling Analysis.....	4
3.1.2 Nonlinear Inelastic Buckling Analysis	7
3.2 Steel H-Piles with Concrete Encasement	15
3.2.1 Linear Buckling Analysis	15
3.2.2 Nonlinear Buckling Analysis.....	16
3.3 Eccentric Loads on Steel H-piles with Concrete Encasement.....	20
CHAPTER 4: PILE ASSESSMENT TOOL.....	24
4.1 Introduction	24
4.2 Pile Bents with Concentric Loads	27
4.3 Pile Bents with Eccentric Loads.....	34
4.4 Pile Assessment Tool Development.....	46
CHAPTER 5: SUMMARY AND CONCLUSIONS	53
REFERENCES	55

LIST OF FIGURES

Figure 3.1 Dimensions and boundary conditions of the example pile.....	5
Figure 3.2 FE model and controlled buckling mode of the example pile.....	6
Figure 3.3 Bilinear residual stress distribution	9
Figure 3.4 FE model of the example pile.....	10
Figure 3.5 Residual stress in flanges and web of the pile	12
Figure 3.6 Stress in the FE model at failure.....	14
Figure 3.7 Load-deflection relationship for the FE model	15
Figure 3.8 FE model and controlled buckling mode of the example pile with concrete encasement	16
Figure 3.9 Z-stress in the FE model at failure	19
Figure 3.10 Load-deflection relationship for the FE model	20
Figure 3.11 FE model with eccentric loads	21
Figure 3.12 FE model with different crack modeling techniques.....	22
Figure 3.13 Z-stress contours of different FE models	23
Figure 4.1 Pile bent with encased piles.....	24
Figure 4.2 Important parameters for the pile bent	26
Figure 4.3 Buckling strength of steel H-piles with different concrete encasement lengths under concentric loads.....	33
Figure 4.4 Buckling strength of steel H-piles with different concrete encasement lengths under eccentric loads.....	45
Figure 4.5 Comparisons between the pile strengths derived from the AISC equations and FE results – concentric loads/no concrete encasement	47
Figure 4.6 Comparisons between the pile strengths derived from the AISC equations and FE results – eccentric loads/no concrete encasement	48
Figure 4.7 Calibrated buckling strength of steel H-piles with different concrete encasement lengths under eccentric loads	51
Figure 4.8 Graphical user interface of the pile assessment tool	52

LIST OF TABLES

Table 4.1 Permissible dimensions for steel H-pile sections – Iowa P10L standards.....	25
Table 4.2 FE models with different combinations of unbraced pile length and concrete encasement length – HP10×42.....	27
Table 4.3 FE models with different combinations of unbraced pile length and concrete encasement length – HP10×57.....	27
Table 4.4 FE models with different combinations of unbraced pile length and concrete encasement length – HP12×53.....	27
Table 4.5 FE models with different combinations of unbraced pile length and concrete encasement length – HP14×73.....	28
Table 4.6 FE models with different combinations of unbraced pile length and concrete encasement length – HP14×89.....	28
Table 4.7 Comparisons of steel H-piles with no concrete encasements – HP10×42.....	29
Table 4.8 Comparisons of steel H-piles with no concrete encasements – HP10×57.....	29
Table 4.9 Comparisons of steel H-piles with no concrete encasements – HP12×53.....	29
Table 4.10 Comparisons of steel H-piles with no concrete encasements – HP14×73.....	30
Table 4.11 Comparisons of steel H-piles with no concrete encasements – HP14×89.....	30
Table 4.12 Combined axial compression and flexure calculations including flexural resistance about strong axis – HP10×42	38
Table 4.13 Combined axial compression and flexure calculations including flexural resistance about weak axis of the piles under eccentric loads – HP10×42	38
Table 4.14 Combined axial compression and flexure calculations including flexural resistance about strong axis of the piles under eccentric loads – HP10×57	39
Table 4.15 Combined axial compression and flexure calculations including flexural resistance about weak axis of the piles under eccentric loads – HP10×57	39
Table 4.16 Combined axial compression and flexure calculations including flexural resistance about strong axis of the piles under eccentric loads – HP12×53	40
Table 4.17 Combined axial compression and flexure calculations including flexural resistance about weak axis of the piles under eccentric loads – HP12×53	40
Table 4.18 Combined axial compression and flexure calculations including flexural resistance about strong axis of the piles under eccentric loads – HP14×73	41
Table 4.19 Combined axial compression and flexure calculations including flexural resistance about weak axis of the piles under eccentric loads – HP14×73	41
Table 4.20 Combined axial compression and flexure calculations including flexural resistance about strong axis of the piles under eccentric loads – HP14×89	42
Table 4.21 Combined axial compression and flexure calculations including flexural resistance about weak axis of the piles under eccentric loads – HP14×89	42

ACKNOWLEDGMENTS

The authors would like to thank the Iowa Department of Transportation (DOT) for sponsoring this research and the Federal Highway Administration (FHWA) for state planning and research funding.

EXECUTIVE SUMMARY

The Iowa Department of Transportation (DOT) rating engineer is sometimes asked by field personnel to make quick decisions regarding bridge pile capacity and stability when scour is identified around pile bents. This is because the unbraced lengths of the piles increase when scour removes a certain amount of soil around the piles. The resulting increase in the unbraced lengths of the piles has a negative impact on the actual capacity and stability of these piles.

Codified specifications and manuals do not address the concrete encasement around the piles, despite the fact that the stiffness of the concrete encasement makes a significant positive contribution to pile capacity and stability. To quickly make decisions regarding pile capacity and stability based on manual calculations, the rating engineer needs to make multiple, on-the-fly assumptions. Furthermore, due to the complexities in estimating the remaining capacity in these atypical situations, the rating engineer must sometimes make conservative assumptions in the interest of providing timely responses. If practitioners are asked, to provide timely, realistic estimations of pile capacity and stability, it is desirable to take into account both the increase in pile unbraced lengths due to scour and the influence of the stiffness of the concrete encasements in making these critical decisions.

To evaluate the capacity of steel H-piles with concrete encasements, the research team developed and implemented a numerical evaluation program. The program consists of various types of finite element (FE) models established using appropriate FE modeling techniques. To validate these techniques, the researchers established FE models for steel H-piles without concrete encasement and then for steel H-piles with concrete encasement and, where possible, compared them to known/published capacities.

To provide flexibility in use of the research results, load eccentricities were also taken into account in the validated FE models. It is worth noting that geometric imperfection (out-of-straightness) and residual stress were included in the nonlinear FE models, which is consistent with the specifications in the American Institute of Steel Construction (AISC) Steel Construction Manual (AISC 2017). The researchers validated the FE models against the results calculated from the provisions of the AISC Steel Construction Manual.

After validating the FE modeling techniques, the research team performed parametric studies to understand the influence of concrete encasement on pile capacity. The individually encased pile bents in the P10L standard, which are in the current Iowa design standard for pile bents with steel H-piles, were utilized for the parametric studies. Five H-pile sections (HP10×42, HP10×57, HP12×53, HP14×73, and HP14×89) were considered for the parametric studies. Additionally, the parametric studies were designed to take into account different combinations of unbraced pile length and concrete encasement length.

The buckling strength of the steel H-piles with concrete encasement was evaluated under two different loading conditions (i.e., concentric and eccentric loading conditions). Based on the results from the parametric studies, the relationships of the buckling strength of the steel H-piles with concrete encasement lengths were plotted for the five cross-sections and two loading

conditions. Since the buckling strength of the steel H-piles without concrete encasement under eccentric loads was conservatively estimated by the AISC Steel Construction Manual (AISC 2017), the buckling strength of the steel H-piles with concrete encasements under eccentric loads derived from FE results was calibrated to achieve a safety margin similar to that in the AISC Steel Construction Manual.

Given that the stiffness contribution of concrete encasements is not taken into account by the AISC Steel Construction Manual or the American Association of State Highway and Transportation Officials (AASHTO) load and resistance factor design (LRFD) specifications (AASHTO 2015) for estimating the buckling strength of steel H-piles with concrete encasements, the researchers developed a pile assessment tool to quickly calculate the buckling strength of steel H-piles with concrete encasements. The tool includes the relationship of the buckling strength of the steel H-piles with the concrete encasement lengths for five cross-sections and two loading conditions. For the user's convenience, the researchers developed a graphical user interface for the pile assessment tool to quickly estimate the pile buckling strength. The tool requires users to input four parameters:

- Loading eccentricity (e)
- H-pile section type (HP10×42, HP10×57, HP12×53, HP14×73, or HP14×89)
- Unbraced pile length (L_p)
- Concrete encasement length (L_c)

This pile assessment tool can be utilized to quickly calculate pile capacity and to assist state rating engineers in making rapid decisions on pile capacity and stability.

CHAPTER 1: INTRODUCTION

1.1 Background

From time-to-time, the Iowa Department of Transportation (DOT) rating engineer is called on by field personnel during flood events to make quick decisions regarding bridge closures when significant scour around pile bents is identified.

When scour removes soil from around the piles, the unbraced lengths of the piles increase. This increase of unbraced length has a negative impact on the actual capacity and stability of these piles. On the other hand, the concrete encasements around piles is ignored in the pile bent design and by the codified specifications and manuals while the stiffness of the concrete encasements has a positive contribution to pile capacity and stability.

To quickly make decisions regarding pile capacity and stability based on manual calculations, the rating engineer has historically had to make multiple, on-the-fly assumptions. Due to complexities in estimating remaining capacity in these atypical situations, the rating engineer must sometimes make conservative assumptions in the interest of providing timely responses. If practitioners are asked to provide timely, realistic estimations of pile capacity and stability, it is desirable to take into account both the increase in pile unbraced lengths and the influence of the stiffness of the concrete encasements.

1.2 Objective and Scope

The main objective of this work was to develop a tool to quickly assess pile capacity while taking into account the varying unbraced pile lengths and the stiffness contribution of their concrete encasements. To achieve this goal, the research team developed and implemented a numerical program consisting of hundreds of finite element (FE) models to characterize the influence of the unbraced pile lengths as well as their concrete encasements on pile capacity. Based on the simulation results, the researchers then created a pile assessment tool to calculate pile capacity and assist in making rapid decisions related to pile capacity.

In fact, the rating engineer could establish the maximum permissible amount of scour for each pile bent prior to any flood event since the tool is relatively easy to use.

1.3 Work Plan

Task 1 – Literature Review and Other Information Collection

A literature review was conducted on rapid assessment of pile capacity and stability. Previous similar work related to the Iowa DOT's P10L standard uncovered very little literature on this topic. When possible, information/tools/approaches in use in other states were obtained, critiqued, and summarized.

Task 2 – Development of Assessment Tool

Following information collection, the research team worked with the rating engineer to fully define the parameters that needed to be included in the assessment tool. To incorporate a stepped column into the tool, the research team needed to consider inelastic buckling. This portion of the investigation consisted of the development of nonlinear FE models that were used to predict the buckling behavior in the inelastic region.

To ensure a wide range of applicability, the researchers completed a broad parametric study that considers multiple combinations of stiffness and level of exposure (i.e., scour). Once they developed a complete approach, the team converted it into a usable tool.

Task 3 – Documentation and Information Dissemination

The work completed for this project is summarized in this final report.

CHAPTER 2: LITERATURE REVIEW

Scour is defined by the USDA Forest Service as “the erosion or removal of streambed or bank material from bridge foundations due to flowing water” (Kattell and Eriksson 1998), and it causes 60% of bridge failures in the US (Lagasse et al. 2007). Scour removes material from around bridge piles and influences the boundary conditions and unbraced lengths of the piles. Accordingly, the influence of scour on the strength and stability of piles must be evaluated whenever scour is suspected.

The behavior of compression members has been investigated for more than 250 years. Except for short columns, which can sustain loads up to yield stress levels, stability dominates the strength of most compression members. Column buckling theory was initially introduced by Leonhard Euler in 1759. However, Euler’s approach is not always applicable to the design of actual columns because not all possible failure modes are taken into account. Actually, Euler’s approach can only be used to calculate the buckling strength of columns with large slenderness ratios. To evaluate the actual buckling strength of compression columns, steel yielding, local buckling, residual stress, imperfection (out-of-straightness), and load eccentricity should be taken into account (Salmon and Johnson 1996).

Since experimental work to characterize the strength of columns is generally expensive, numerical simulation offers a more cost-effective approach to develop relationships for estimating the strength and stability of columns. However, numerical simulations also possess some limitations, and limited research has been conducted to evaluate the strength of eccentrically loaded steel columns with concrete encasements.

One example of related research, conducted by Ellobody et al. (2011), established three-dimensional (3D) FE models to evaluate the strength of eccentrically loaded concrete encased steel composite columns. The FE models accounted for the load eccentricity, initial overall geometric imperfection, and the inelastic behavior of materials. The column strengths predicted from the FE models compared well to the code specifications (i.e., Eurocode4). However, only the behavior of full-length encased steel columns was studied. The results of this study provide a good understanding of modeling approaches but the results are not directly applicable because scour also affects partial-length concrete encasements (i.e., stepped columns).

CHAPTER 3: NUMERICAL EVALUATION PROGRAM

In order to develop a sound numerical evaluation program, FE models should be established using appropriate FE modeling techniques. These techniques should be validated against available resources (e.g., American Institute of Steel Construction [AISC] Steel Construction Manual [AISC 2017]) where possible. To provide validation of the FE modeling techniques, FE models were first established for the following:

1. Linear elastic buckling analysis
2. Non-linear elastic buckling analysis with initial consideration of steel H-piles without concrete encasements
3. Steel H-piles with concrete encasements

The aim was to first validate the adequacy of simple FE models and then proceed with more complicated FE models. Finally, load eccentricities were taken into account in the validated FE models. The FE model validation process was conducted as follows.

3.1 Steel H-Piles without Concrete Encasement

In order to develop sound FE models for the study, the FE models of steel H-piles without concrete encasements were first established. The idea was that the necessary procedures for the buckling analysis would first be understood using simpler FE models and then the procedures would be utilized for more complicated FE models. The linear and non-linear buckling analyses were performed and the adequacy of the FE models was validated against the capacity predictions of steel H-piles using Euler's buckling equation and codified equations from the AISC Steel Construction Manual (AISC 2017).

3.1.1 Linear Elastic Buckling Analysis

Linear elastic buckling analysis, also called the eigenvalue buckling analysis, can be utilized to derive the theoretical buckling strength of an ideal column (and the bifurcation point). The predicted capacity should be equal to the classical Euler's buckling strength. In this study, linear elastic buckling analysis was used only to validate the FE modeling techniques and buckling analysis procedures. In reality, due to the geometric imperfections and residual stress, the buckling strength of a column is always less than the classical Euler's buckling strength, and non-linear elastic buckling analysis should be utilized to obtain the actual strength of piles with or without concrete encasements.

An HP10×42 pile section was used as an example to demonstrate the simulation process as shown in Figure 3.1.

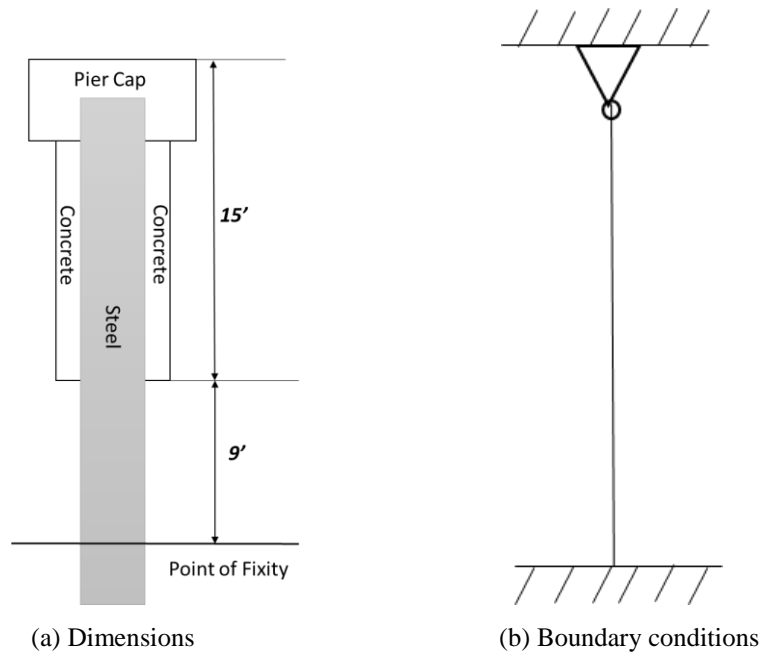


Figure 3.1 Dimensions and boundary conditions of the example pile

In the example, the total unbraced length is 24 ft, and the concrete encasement length is 15 ft (the concrete encasement consisting of a 16×16 in. square section was not considered during initial analysis procedure development) with pinned and fixed boundary conditions at the top and bottom of the unbraced pile model, respectively. Regardless of the type of pier cap (monolithic or non-monolithic), the top of the pier cap should be used to establish the pile dimensions.

This example represents a common situation for pile bents in Iowa. Normally, the concrete encasement extends 3 ft below the natural streambed to protect the pile from impact damage due to large debris (e.g., tree limbs) and ice flowing downstream. The concrete encasement also provides corrosion resistance to the pile. In flood situations, scour erodes the streambed soil resulting in a larger unbraced length. The actual point of pile fixity is always some distance below the streambed surface (natural or scoured).

A 3D linear elastic FE model was established for the buckling analysis as shown in Figure 3.2(a).

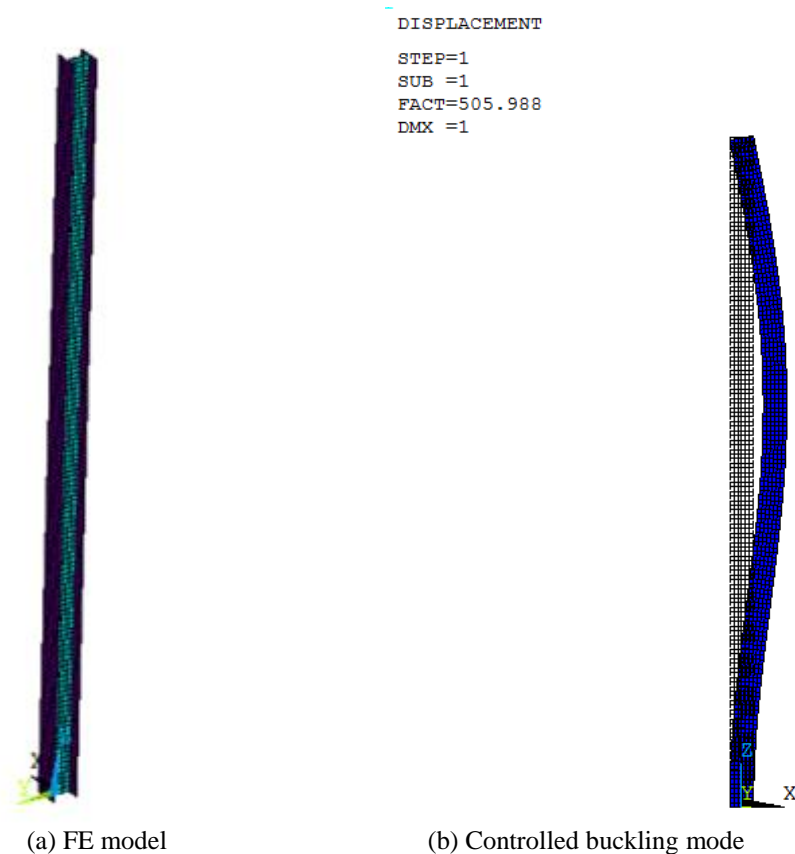


Figure 3.2 FE model and controlled buckling mode of the example pile

Concrete was not included in the FE model. The flanges and web of the steel column were both modeled using a four-noded shell element with three translational and three rotational degrees of freedom at each node. An elastic uniaxial material model was used for the steel. The elastic modulus and Poisson's ratio of the steel were set to 29,000 ksi and 0.3, respectively. A compression force of 1 kip was applied to the top of the column. Pinned and fixed boundary conditions were assigned at the top and bottom of the FE model, respectively.

Prestress effects were activated to calculate the stress stiffness matrix used to derive the eigenvalues of the structure under an applied loading condition. The eigenvalues are also referred to as buckling load factors and each eigenvalue is associated with a different buckling mode. Commonly, the lowest load factor is of interest and, for this study, the flexural buckling mode with respect to the weak axis is the controlling buckling mode.

The predicted buckling load is derived by the product of the load factor of interest (commonly, the lowest load factor) and the applied compression force. Buckling mode shapes can be displayed to select the buckling model of interest for the analysis. As shown in Figure 3.2(a), the lowest load factor is 506, and the weak-axis flexural buckling strength is 506 kips (i.e., the product of 506 and 1 kip).

According to the AISC Steel Construction Manual (AISC 2017), the buckling strength of the pile without slender elements is determined by:

$$P_c = F_{cr} A_g \quad (1)$$

The flexural buckling stress, F_{cr} is derived by:

(a) When $\frac{KL}{r} \leq 4.71 \sqrt{\frac{E}{F_y}}$, (or $F_e \geq 0.44F_y$)

$$F_{cr} = \left[0.658^{\frac{F_y}{F_e}} \right] F_y \quad (2)$$

(b) When $\frac{KL}{r} > 4.71 \sqrt{\frac{E}{F_y}}$, (or $F_e < 0.44F_y$)

$$F_{cr} = 0.877F_e \quad (3)$$

where F_e = elastic critical buckling stress is determined by:

$$F_e = \frac{\pi^2 E}{\left(\frac{KL}{r} \right)^2} \quad (4)$$

The buckling strength of the pile per the AISC equations was calculated to be 505 kips (values for F_y , K , and r for various pile geometries and combinations are shown later in Tables 4.7 through 4.10), which is almost equal to that predicted by the FE model. Based on these and other similar results, the adequacy of the FE model and the linear elastic buckling analysis procedure that the researchers developed were validated.

3.1.2 Nonlinear Inelastic Buckling Analysis

A nonlinear buckling analysis was performed by gradually increasing the applied loads until reaching a load level at which the structure becomes unstable. A perfect elastic–plastic uniaxial material model including bilinear kinematic hardening was used for the steel. And, an initial geometric imperfection (out-of-straightness) and residual stress were applied to the FE model to reflect the initial condition of a real column.

Geometric Imperfection (Out-of-Straightness)

For nonlinear inelastic buckling FE simulation, a geometric imperfection needs to be applied to the FE model in order to activate the inelastic buckling mode. Per Salmon and Johnson (1996), based on statistical data from measurements of real columns, the initial out-of-straightness of the real columns ranges from $L/2000$ to $L/1000$. And, per the AISC Steel Construction Manual (AISC 2017), the AISC equations were developed based on an initial out-of-straightness of $L/1470$. Because the AISC equations were utilized to validate FE models, an initial out-of-straightness of $L/1470$ was assigned to the FE models. Geometric imperfection does not include cases where a battered pile is suspected of having non-axial loads applied (with or without eccentricities).

Two approaches (i.e., linear buckling mode and eccentric loads) can be used to add the initial out-of-straightness of an FE model. The first approach is to derive the linear buckling mode of interest by performing a linear buckling analysis. Once that is determined the initial out-of-straightness is assigned to the FE model based on the linear buckling mode and the maximum initial out-of-straightness of $L/1470$. Essentially, this method “pre-bent” the pile in a shape that would lead to earlier buckling (i.e., lower buckling loads). The second approach is to incorporate the initial out-of-straightness of $L/1470$ via an eccentric load (with an eccentricity of $L/1470$) at the top of a pile.

Following preliminary FE simulations using the two approaches, the researchers found that the two approaches resulted in almost identical predicted buckling strength of a pile. For simplicity of performing FE simulations, the second approach of using eccentric loads was adopted in the FE models for the study. Note that the 2 in. of eccentricity was considered to be about both axis simultaneously.

Residual Stress

Residual stresses are induced in steel members during the process by which steel blanks are formed into a steel section (Salmon and Johnson 1996). The residual stresses associated with plastic deformation are caused by several sources: uneven cooling, cold bending, punching and cutting operations, and welding. For hot-rolled sections, the flanges cool more slowly than the web region and the flange tips exposed to the air cool more rapidly than the junction of flanges and the web. Accordingly, compressive residual stresses exist at flange tips and mid-depth of the web, while tensile residual stresses exist in the junction of the flanges and web (Salmon and Johnson 1996).

Abambres and Quach (2016) conducted a comprehensive literature review on research related to residual stress distribution in steel members. For bisymmetric I and H sections, residual stress had been measured by many researchers (e.g., Huber 1956, Beedle and Tall 1960, Alpsten 1968). A bilinear residual stress distribution in flanges and a symmetric distribution along the web for hot-rolled I and H sections were proposed by Galambos and Ketter (1959). A parabolic residual stress distribution in the flanges and web for hot-rolled I and H sections was proposed by Young (1972). A bilinear residual stress distribution in the flanges and web for hot-rolled I and H

sections was adopted by the European Convention for Constructional Steelwork (ECCS 1984) and in the Swedish design code (BSK 99 2003). The bilinear residual stress distribution was used for both the flanges and web as shown in Figure 3.3 (f_y is the material yield stress and α is 0.3, negative in compression).

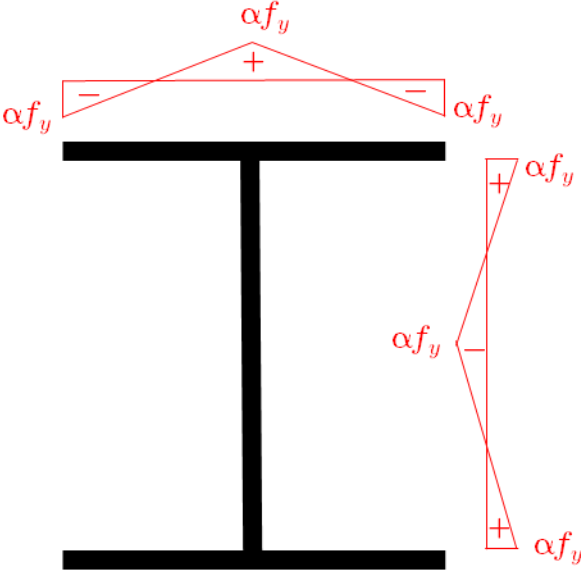


Figure 3.3 Bilinear residual stress distribution

FE Simulations

The example pile in Section 3.1.1 was further utilized to validate the nonlinear buckling analysis technique. A three-dimensional elastic-plastic FE model was established for the analysis as shown in Figure 3.4.

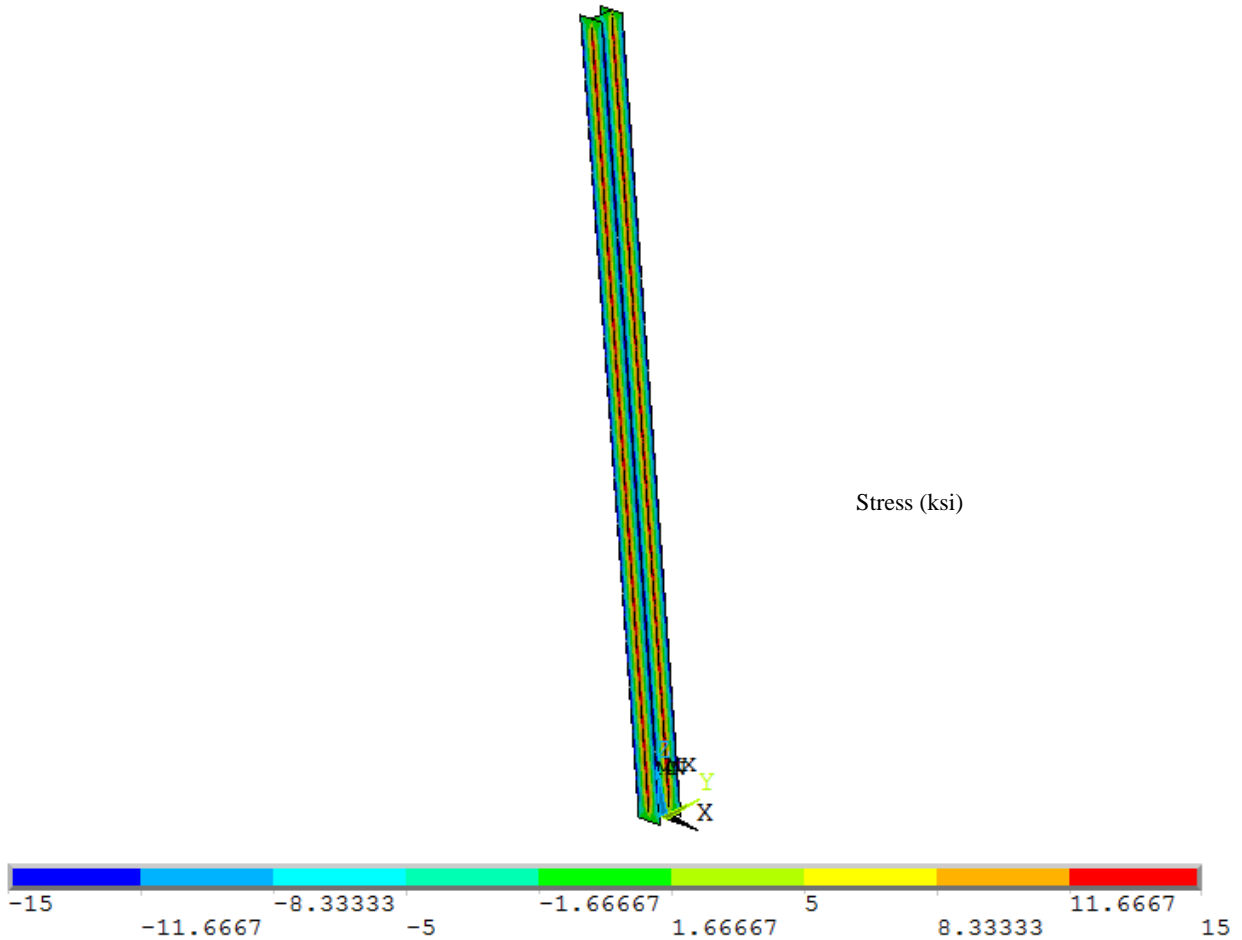


Figure 3.4 FE model of the example pile

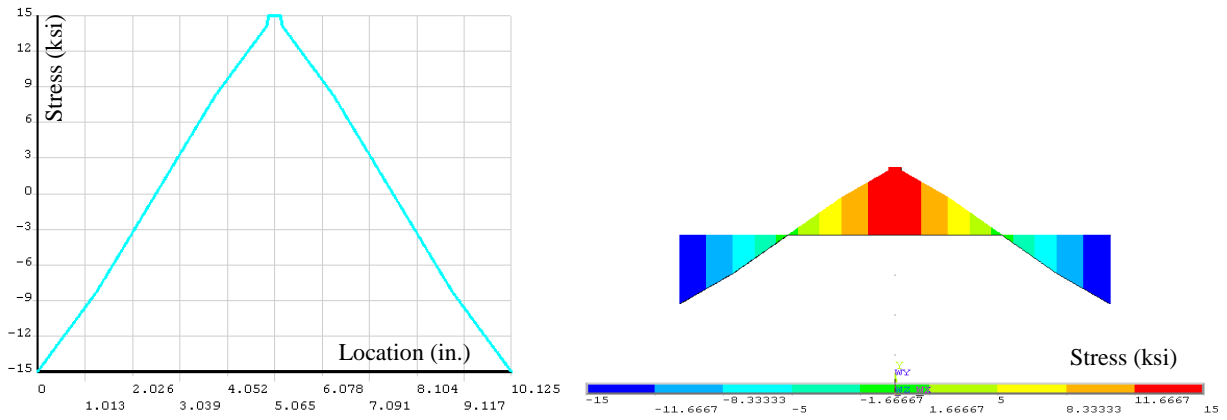
The flanges and web of the steel column were both modeled using a four-noded shell element with three translational and three rotational degrees of freedom at each node. A perfect elastic-plastic material model was used for the steel. The elastic modulus, strain hardening modulus, and Poisson's ratio of the steel were set to 29,000 ksi, 0, and 0.3, respectively.

As mentioned previously, the bilinear residual stress distribution shown in in Figure 3.3 was used for both the flanges and the web. The material yield stress and α , are 50 ksi and 0.3 and the maximum residual stress is 15 ksi.

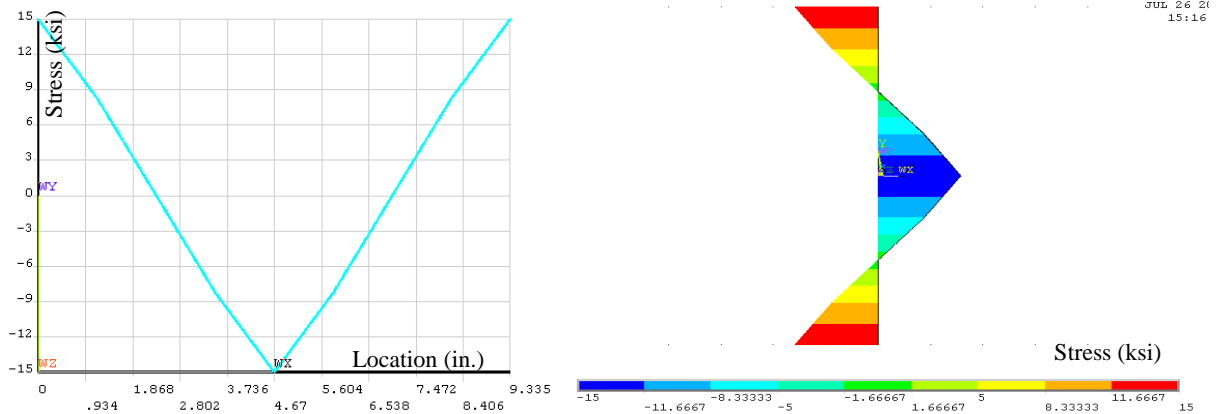
The command "Initial State" was utilized to apply the residual stress to the FE model. Note that the term "Initial State" means the state of a structure at the start of an analysis when the structure has not been deformed and stressed. (ANSYS 2012). The appropriate initial stresses were assigned to all the nodes of the FE model to generate the desired bilinear residual stress distribution in the FE model as shown in Figure 3.5(a).



(a) Residual stress contour in the FE model



(b) Residual stress distribution in flanges



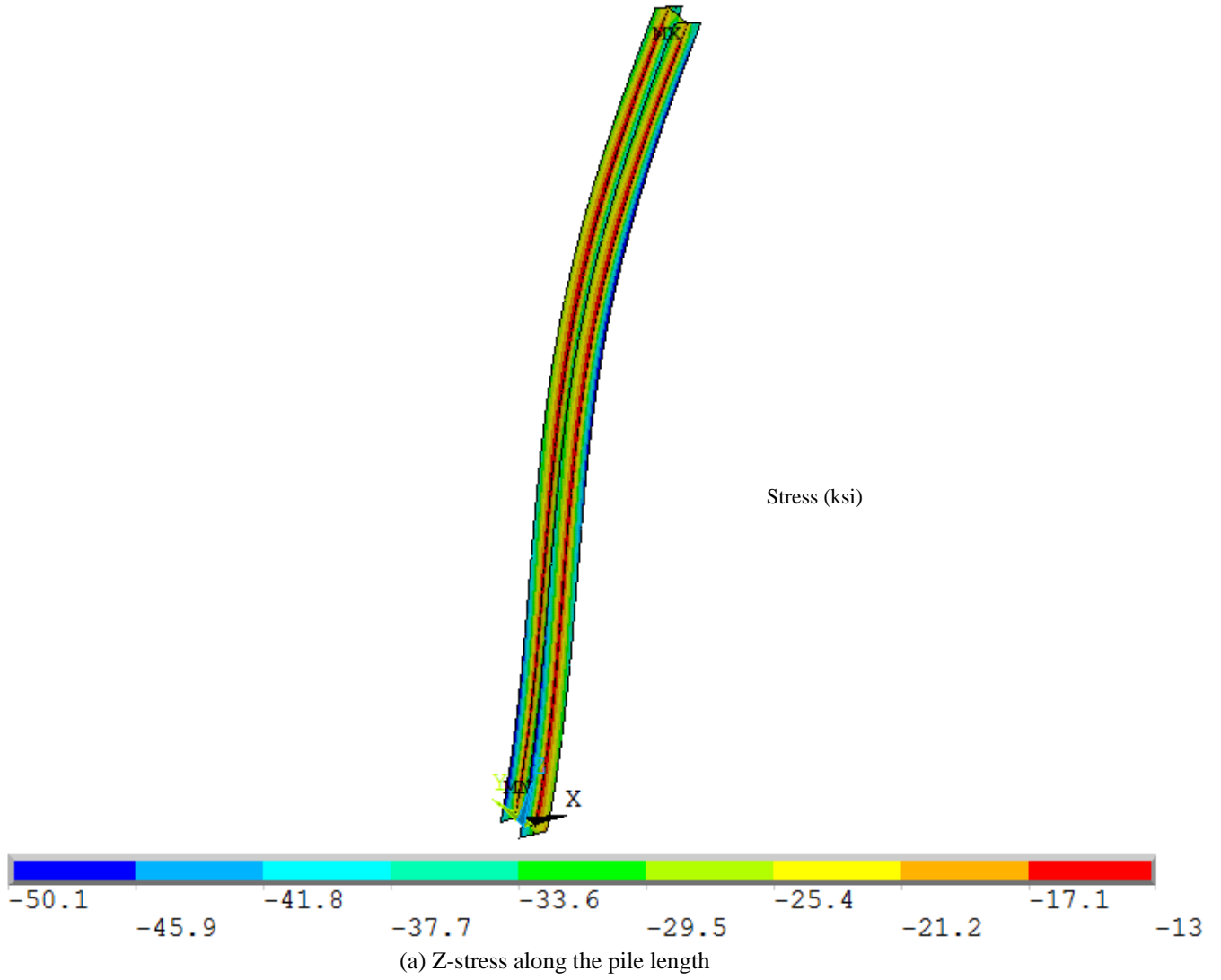
(c) Residual stress distribution in web

Figure 3.5 Residual stress in flanges and web of the pile

The desired bilinear residual stress distribution from -15 to 15 ksi (negative in compression) was generated in the flanges and web as shown in Figure 3.5(b) and Figure 3.5(c).

After the residual stress had been assigned to the FE model, a group of compression forces was applied to the top nodes of the FE model to create a load with an eccentricity of $L/1470$. Note that the load eccentricity was utilized to take into account the geometric imperfection (out-of-straightness). The previously discussed pinned and fixed boundary conditions were assigned at the top and bottom of the FE model, respectively. The default convergence criteria and tolerances for the computation convergence were used in the analysis. Large-deflection effects were included, stress stiffness effects were activated, and automatic load stepping was used in the nonlinear analysis.

The load gradually increased until buckling failure of the column occurred. Just prior to the failure of the column, the Z-stress along the pile length and von-Mises stress were extracted; these are plotted in Figure 3.6(a) and Figure 3.6(b), respectively.



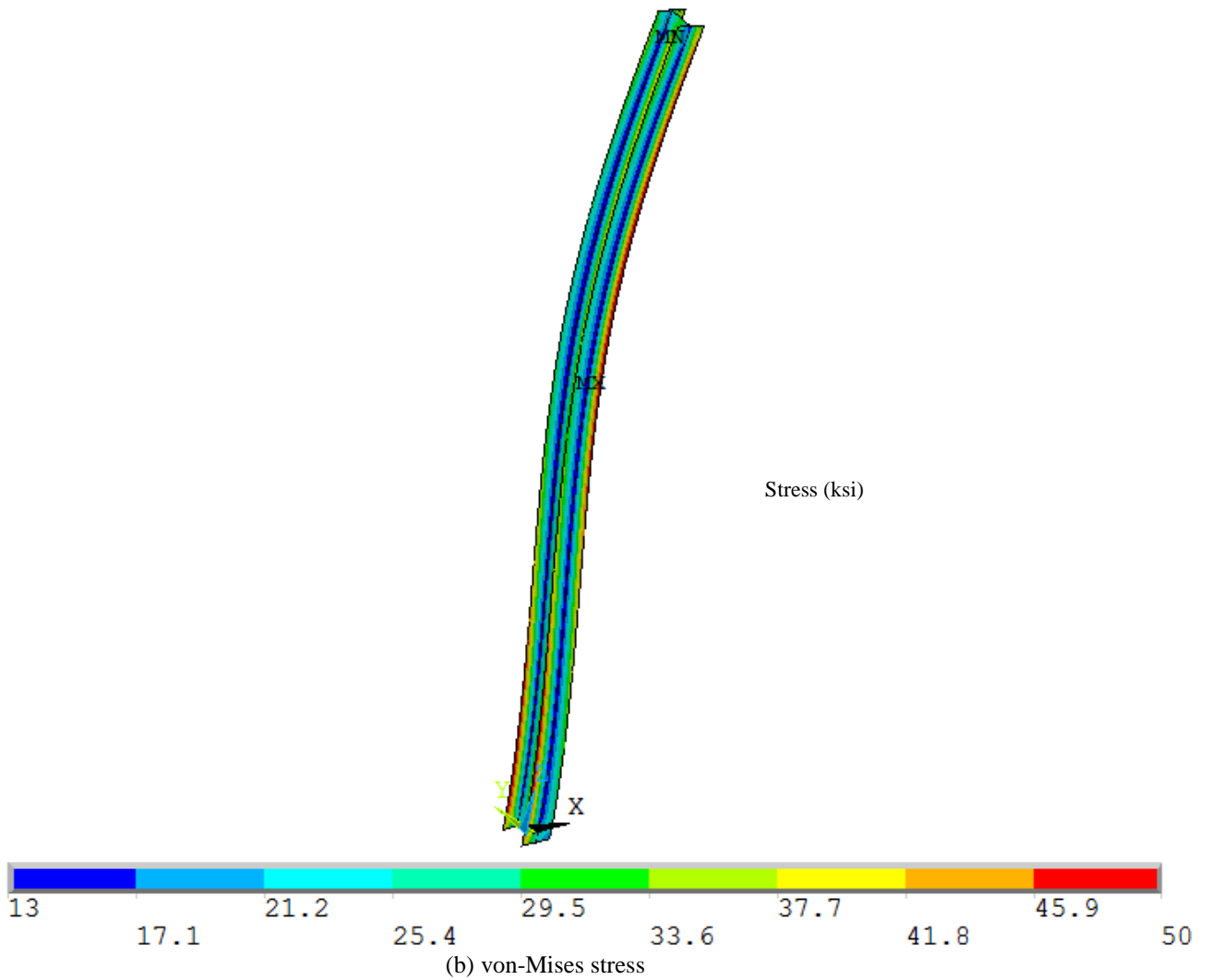


Figure 3.6 Stress in the FE model at failure

As shown in Figure 3.6, the maximum stress is located at the tips of the flanges; the Z-stress could go slightly higher than the yield stress of 50 ksi, while the von-Mises stress can only rise to 50 ksi due to the three-dimensional stresses used in the FE model.

When approaching the failure point, the deflection of the column increased significantly while the load did not change at all, as shown in Figure 3.7.

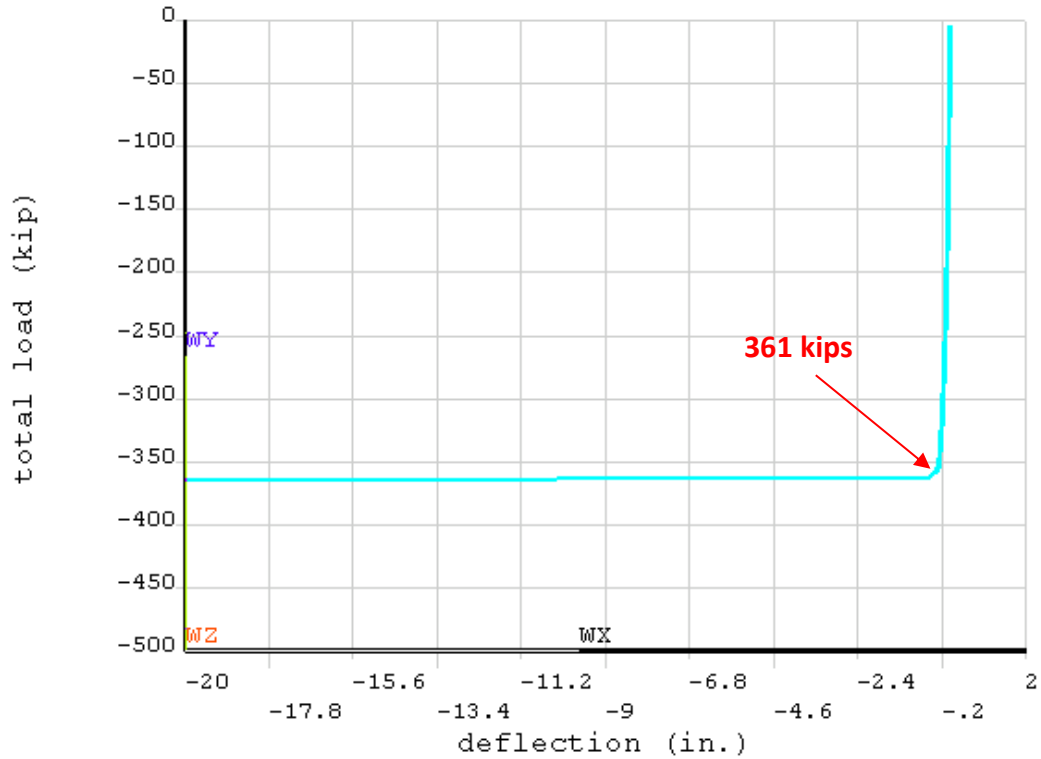


Figure 3.7 Load-deflection relationship for the FE model

The maximum load (i.e., the buckling load) that the column can take during the loading process is considered to be the buckling strength of the column. According to the AISC Steel Construction Manual (AISC 2017), the buckling strength of the example pile can be estimated by Equation (2) and is equal to 370.9 kips, which is slightly larger than that predicted by the FE model. Therefore, the adequacy of the FE model for a pure steel pile through nonlinear buckling analysis was validated against the pile capacity estimated by the AISC equations (AISC 2017).

3.2 Steel H-Piles with Concrete Encasement

After the adequacy of the linear elastic buckling analysis and nonlinear buckling analysis procedures were validated via comparison with the estimates from classical Euler's buckling analysis and AISC equations, respectively, the general analysis techniques were further developed to include the concrete encasement in the FE model. The buckling strength of steel H-piles with concrete encasement can then be determined through a similar buckling analyses.

3.2.1 Linear Buckling Analysis

The previously used three-dimensional linear elastic FE model was updated to include concrete for the buckling analysis as shown in Figure 3.8(a).

The previous example pile shown in Figure 3.1 was further utilized for demonstration, validation, and further study. The H-pile section, HP10×42, with a total unbraced length of 24 ft, concrete encasement length of 15 ft, and the concrete square section of 16×16 in. were all considered. The steel H-pile was modeled using the techniques described in Section 3.1.2. The encased concrete was modeled using an eight-noded solid element which has three translational degrees of freedom at each node and incorporates cracking and crushing capabilities. The concrete material properties were assigned with multi-linear isotropic hardening in combination with the von Mises yield criterion. The stress-strain relationship of the concrete proposed by Hognestad (1951) was utilized for the concrete constitutive model:

$$f_c = f_c' \left[2 \left(\frac{\varepsilon}{\varepsilon_o} \right) - \left(\frac{\varepsilon}{\varepsilon_o} \right)^2 \right] \quad (6)$$

where, f_c and ε are stress and strain on concrete, respectively; and strain at peak stress (ε_o) is expressed as (Wee et al. 1996):

$$\varepsilon_o = 0.00126(f_c')^{1/4} \quad (\text{in ksi}) \quad (7)$$

The smeared fixed crack model and Rankine maximum stress criterion were utilized to determine the initiation and development of concrete cracking. According to the American Association of State Highway and Transportation Officials (AASHTO) load and resistance factor design (LRFD) specifications (AASHTO 2015), maximum concrete tensile strength can be derived from:

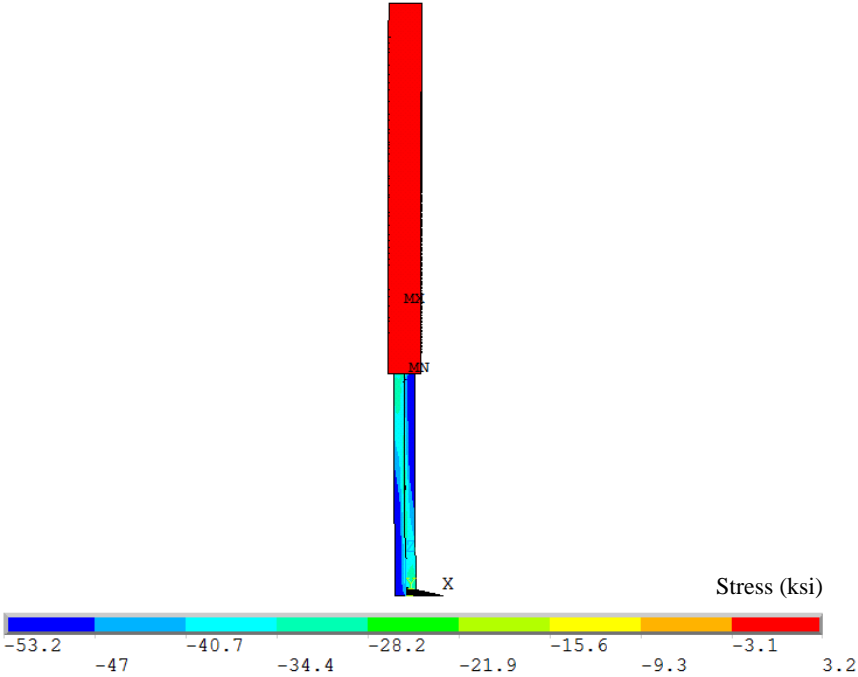
$$f_t = 0.24\sqrt{f_c'} \quad (\text{in ksi}) \quad (8)$$

The concrete element was perfectly connected to the steel H-pile through sharing common nodes. The previously introduced techniques to take into account the initial geometric imperfection (out-of-straightness) and residual stress were also included in the FE model. After the residual stress had been assigned to the FE model, a group of compression forces was then applied to the top nodes of the FE model to create a load with an eccentricity of $L/1470$. Note that the load eccentricity was utilized to take into account the geometric imperfection (out-of-straightness). The pinned and fixed boundary conditions were assigned at the top and bottom of the FE model, respectively. The load was gradually increased until buckling failure of the column occurred. Note that for these analyses, large-deflection effects were included, stress stiffness effects were activated, and automatic load stepping was used during the nonlinear analysis. Convergence criteria and tolerances were set for the displacement and force.

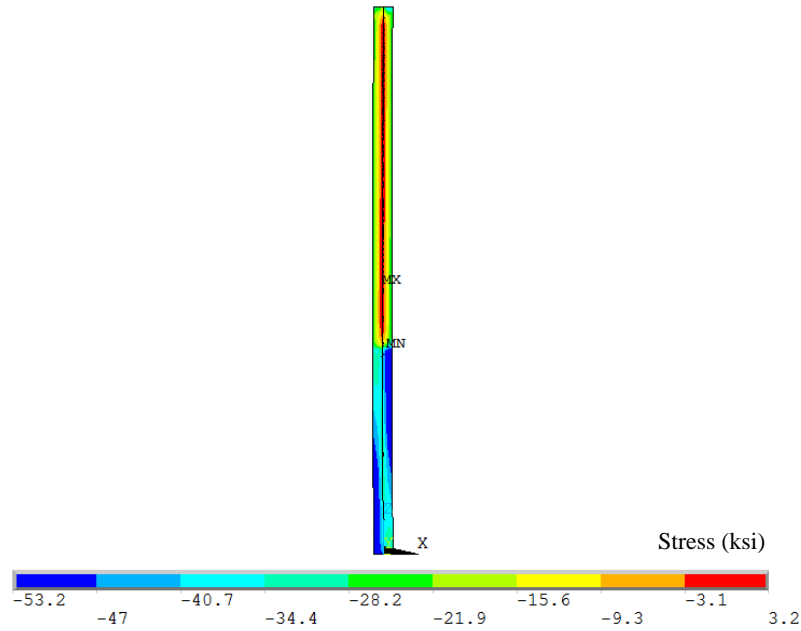
The following strategies were utilized to facilitate convergent computations (Deng et al. 2016a, Deng et al. 2016b, Deng et al. 2016c, Deng et al. 2013, Deng and Morcouis 2013):

- Concrete compressive stress was constrained to a constant value after reaching its peak value
- Shear transfer coefficients of 0.15 and 0.9 were used for open and closed cracks, respectively
- Capability of concrete crushing was deactivated in the analysis, but the failure of the model was determined when the concrete reached the maximum compressive strain of 0.003 (i.e., concrete failure strain)
- Suppression of extra displacement shapes and tensile stress relaxation after cracking were applied to solid elements

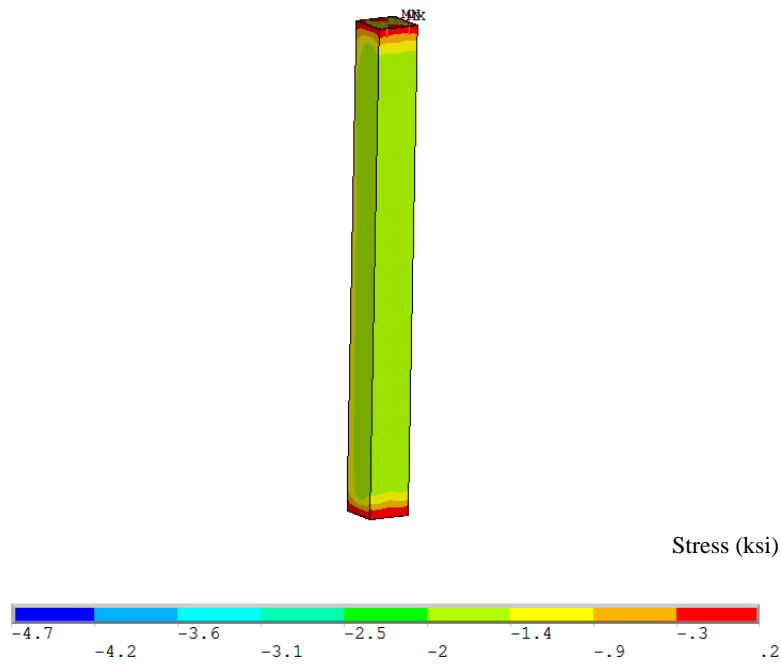
Just prior to the failure of the column, the Z-stress along the pile length in the FE model, in the steel H-pile, and concrete encasement were extracted and subsequently plotted like those shown in Figure 3.9(a), Figure 3.9(b), and Figure 3.9(c), respectively.



(a) Z-stress along the pile length in FE model



(b) Z-stress along the pile length in steel pile



(c) Z-stress along the pile length in concrete

Figure 3.9 Z-stress in the FE model at failure

As shown in Figure 3.9(a) and Figure 3.9 (b), the maximum stress is located at the tips of the flanges of the steel pile; for the pile region encased by the concrete, the stress is reduced significantly due to the force transfer from steel to concrete. Additionally, as shown in Figure 3.9 (c), the stress in the two ends of the concrete encasement is unreasonably large due to the force transfer. This is primarily because the force-slip relationship was not taken into account and stress concentration occurred in the load transfer zone.

When reaching the failure stage, the deflection of the column increased significantly while the load did not change as illustrated in Figure 3.10.

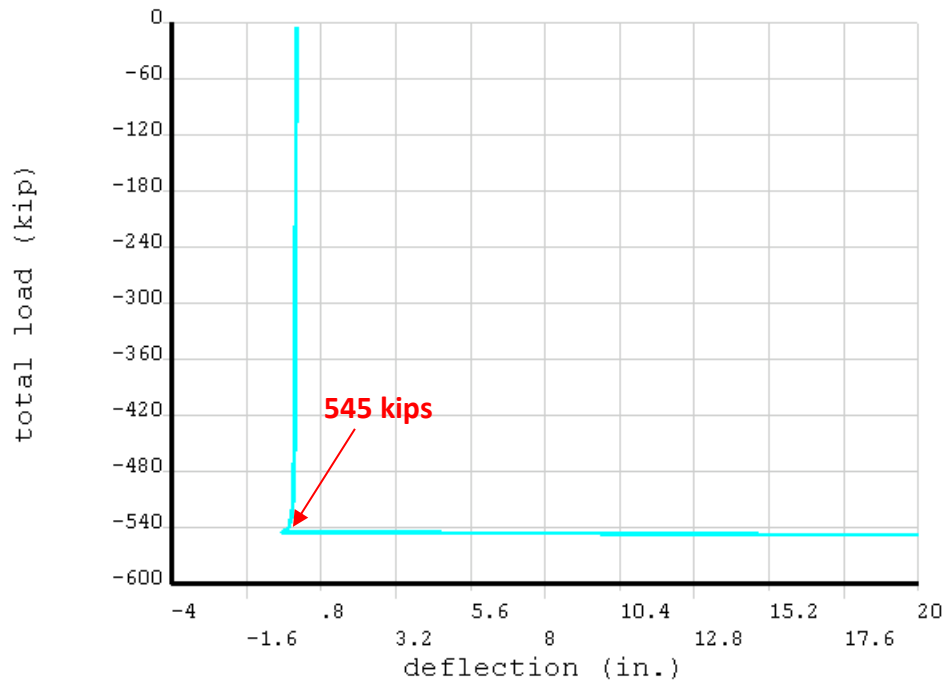


Figure 3.10 Load-deflection relationship for the FE model

The buckling strength of the column is the maximum load that the column can endure during the loading process. The buckling strength of the example pile was determined to be 545 kips by the FE model, which is significantly larger than the rating of 361 kips without any concrete encasement. The results indicate that the stiffness contribution of the concrete encasement can greatly increase the buckling strength of a steel H-pile.

3.3 Eccentric Loads on Steel H-piles with Concrete Encasement

In Iowa, to design or load rate the steel H-piles, the compression load on the top of a pile is assumed to have a 2 in. eccentricity on both axes. The FE model of the example steel pile with concrete encasement from Section 3.3.2 was further utilized to take into account the effects of load eccentricity on the pile buckling strength.

The eccentric loads would tend to induce cracks in the concrete, which in turn reduce the stiffness of the pile member and the pile buckling strength. Two types of FE models were simulated for concrete cracking effect comparison purposes: (1) Model A: FE model with cracking capability concrete and (2) Model B: FE model with cracked concrete killed. Model A was developed using the FE techniques introduced in Section 3.2. Due to the localized effects of the force on the top (inducing cracks), a 1.5 in. steel layer was assigned to the FE model to eliminate the unexpected cracking issues (as shown in Figure 3.11).

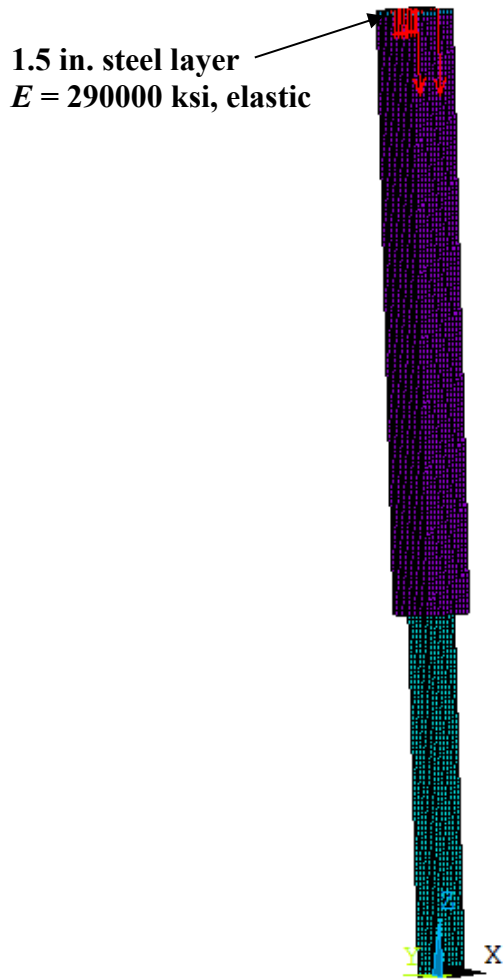


Figure 3.11 FE model with eccentric loads

The eccentric loads were applied on the top of the FE Model A. Model B was a further improvement from model A. After running Model A, the cracked elements were identified in the FE model as shown in Figure 3.12(a).



Figure 3.12 FE model with different crack modeling techniques

For Model B, those cracked elements were killed in the FE model as shown in Figure 3.12(b). Next the eccentric loads were again applied on the top of Model B. For both models, the loads continued to be applied to the FE models until buckling failure occurred.

The buckling loads of models A and B were almost the same, at 456.0 and 454.6 kips, respectively. The Z-stress contours for the two models look similar as shown in Figure 3.13.

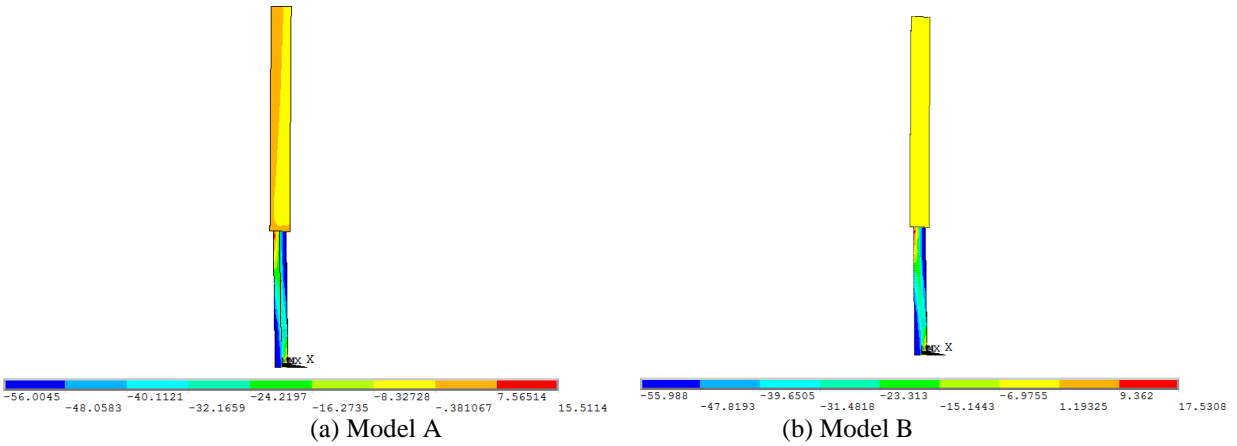


Figure 3.13 Z-stress contours of different FE models

This generally indicated that the two modeling approaches produce the same results when evaluating the buckling strength of steel H-piles with concrete encasement. For simplicity of FE model establishment and computation, the FE simulation techniques used for model A were utilized to predict the buckling strength of the five types of steel H-pile cross-sections.

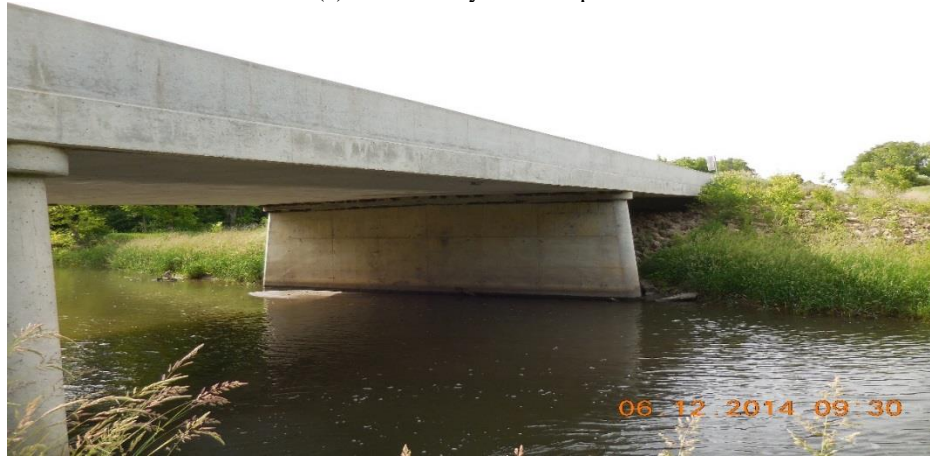
CHAPTER 4: PILE ASSESSMENT TOOL

4.1 Introduction

Different types of bents are considered to be valid for using the results of this study: (1) individually encased pile bents as shown in Figure 4.1(a) and (2) fully encased pile bents as shown in Figure 4.1(b).



(a) Individually encased piles



(b) Fully encased piles

Figure 4.1 Pile bent with encased piles

The basic geometries for individually encased piles are used in the analytical investigation. So, as long as a fully encased pile bent has piles spaced no closer than those used in individual pile bents, the assumption of individual behavior remains conservative. To simplify the scope of work, the individually encased pile bents used in the P10L standard are studied in this research.

Per the P10L standard, five steel H-steel piles are utilized in the design and construction of pile bents as shown in Table 4.1.

Table 4.1 Permissible dimensions for steel H-pile sections – Iowa P10L standards

Steel H-pile Section	Maximum Height (H) (ft)		Recommended Minimum Height (H_{min}) (ft)	Concrete Depth (D_c)	Depth of Fixed Point (D_{FP}) (ft)	Length of Concrete Square (a) (in.)
	Monolithic Cap	Non-Monolithic Cap				
HP10×42	19	15	7	3	6	16
HP10×57	19	16	7			
HP12×53	23	20	9	3	7	18
HP14×73	28	25	13	3	8	20
HP14×89	29	26	13			

D_{FP} – Depth of the fix point below the scoured streambed line; D_c – the concrete depth below the original streambed line; a – the length of the concrete square

In the 1950s, the design standard for pile bents with steel H-piles was known as the P10A standard, which was developed based on the allowable stress design (ASD) method. The computation of pile fixity was determined using the Davisson method (AISC 1986). The computations assumed that the pile head was pinned at the top and fixed at the base and the eccentricity of the axial load was 1 in. on both axes. The potential for scour was neglected in these calculations. These assumptions were found to be unconservative (Iowa DOT 2014).

The current Iowa design standard for pile bents with steel H-piles is the P10L standard, which is based on the LRFD method. Designers are now required to take into account the scour estimates from the hydraulic analysis when determining unbraced pile length. The computation of fixity (which is always some distance below the scour line) used the p-y method, which is programmed in Ensoft’s LPILE software and, in general, verified the Davisson method for this application. The important parameters used for design and load ratings of pile bents are shown in Figure 4.2.

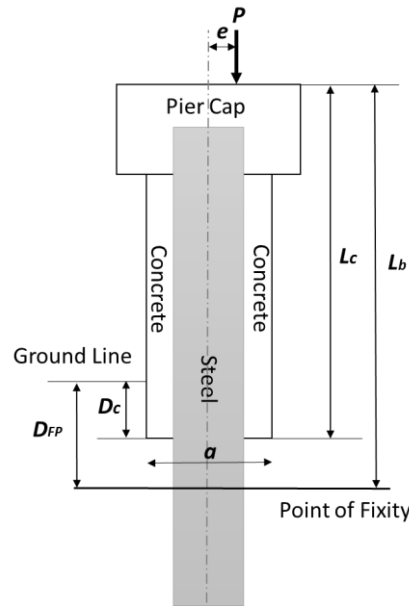


Figure 4.2 Important parameters for the pile bent

The representations of different parameters are as follows. Note that these parameters are in reference to the streambed at the time of evaluation (e.g., the scoured stream bed depth in the case of a post-scour evaluation):

- P is the load on the pile top
- e is the eccentricities on the two axes
- L_p is the pile unbraced length
- L_c is the concrete encasement length
- D_{FP} is the pile depth of the fix point below the current stream-bed/ground line
- D_c is the concrete depth below the current stream-bed/ground line
- a is the width of concrete encasement

Some of those important parameters for the steel H-pile sections are shown in Table 4.1. Commonly, the pile heads are assumed to be pinned at the top and fixed at the bottom. The eccentricity of the axial load is assumed to be 2 in. on both axes. Based on the general study of piles with loads at a 2 in. eccentricity, the permissible dimension of the piles allowed by the P10L standards was determined as shown in Table 4.1. These five H-pile sections and associated dimensions were subsequently used for the finite element simulations and parametric studies described in the next sections. The end-result pile assessment tool was developed based on the results of the parametric studies to quickly estimate the buckling strength of steel H-piles with concrete encasement.

The representations of different parameters are: P is the load on the pile top at the top of the pier cap; e is the eccentricities on the two axes; H and H_{min} are the maximum and minimum lengths, respectively, from the bottom of the pile cap to the scoured streambed line; L_b is the total pile unbraced length; L_c is the concrete encasement length; D_{FP} is the pile depth of the fix point below

the scoured streambed line; D_c is the concrete encasement depth below the original streambed line; a is the width of the sides of the concrete encasement square.

4.2 Pile Bents with Concentric Loads

Based on the permissible dimensions for the five steel H-pile sections shown in Table 4.1, the parameter studies were conducted taking into account the different combinations of the unbraced pile length and the concrete encasement length as shown in Table 4.2 through Table 4.6.

Table 4.2 FE models with different combinations of unbraced pile length and concrete encasement length – HP10×42

Unbraced Pile Length (L_b) (ft)	Concrete Encasement Length (L_c) (ft)
16	0;5;10;13
20	0;5;10;15;17
24	0;5;10;15;18;21
30	0;5;10;15;20;25;27
35	0;5;10;15;20;25;30;32
40	0;5;10;15;20;30;34;37

Table 4.3 FE models with different combinations of unbraced pile length and concrete encasement length – HP10×57

Unbraced Pile Length (L_b) (ft)	Concrete Encasement Length (L_c) (ft)
16	0;5;10;13
20	0;5;10;15;17
24	0;5;10;15;18;21
30	0;5;10;15;20;25;27
35	0;5;10;15;20;25;30;32
40	0;5;10;15;20;30;34;37

Table 4.4 FE models with different combinations of unbraced pile length and concrete encasement length – HP12×53

Unbraced Pile Length (L_b) (ft)	Concrete Encasement Length (L_c) (ft)
19	0;5;10;13;15
25	0;5;10;15;18;21
30	0;5;10;15;20;23;26
35	0;5;10;15;20;25;28;31
40	0;5;10;15;20;25;30;33;36
45	0;5;10;15;20;30;35;38;41

Table 4.5 FE models with different combinations of unbraced pile length and concrete encasement length – HP14×73

Unbraced Pile Length (L_b) (ft)	Concrete Encasement Length (L_c) (ft)
24	0;5;10;15;19
30	0;5;10;15;20;25
35	0;5;10;15;20;25;30
40	0;5;10;15;20;25;30;35
45	0;5;10;15;20;30;35;40
50	0;5;10;15;20;30;35;40;45
55	0;5;10;15;20;30;35;40;45;50
60	0;5;10;15;20;30;35;40;45;50;55

Table 4.6 FE models with different combinations of unbraced pile length and concrete encasement length – HP14×89

Unbraced Pile Length (L_b) (ft)	Concrete Encasement Length (L_c) (ft)
24	5;10;15;19
30	5;10;15;20;25
35	5;10;15;20;25;30
40	5;10;15;20;25;30;35
45	5;10;15;20;30;35;40
50	5;10;15;20;30;35;40;45
55	5;10;15;20;30;35;40;45;50
60	5;10;15;20;30;35;40;45;50;55

Note that the amount of concrete encasement length was typically incremented at around 5 ft and the maximum concrete encasement length was generally set from 3 ft to 5 ft above the fix point. The group of pile lengths for each of the five sections were selected by taking into account different slenderness ratios for intermediate and long columns as shown in Table 4.2 through Table 4.11. Intermediate and long columns were selected for the FE simulations instead of short columns. The cross-sectional area, the moment of inertia, the slenderness ratio, and the limit for the long column are summarized in Table 4.7 through Table 4.11.

Table 4.7 Comparisons of steel H-piles with no concrete encasements – HP10×42

Pile Length (L_b) (ft)	Area (in ²)	Moment of Inertia (in ⁴)	K	KL/r	Limit for Elastic Buckling	FE Results - Nonlinear Analysis (kips)	AISC Equations (kips)	FE Results - Linear Elastic Analysis (kips)	Euler Buckling Strength (kips)	Full Yield Strength (kips)
16	12.4	71.7	0.7	55.9	113.4	492	493	1142	1136	620
20	12.4	71.7	0.7	69.9	113.4	434	434	735	727	620
24	12.4	71.7	0.7	83.8	113.4	361	371	513	505	620
30	12.4	71.7	0.7	104.8	113.4	275	278	329	323	620
35	12.4	71.7	0.7	122.3	113.4	215	208	242	237	620
40	12.4	71.7	0.7	139.7	113.4	174	159	185	182	620

K – a scalar to adjust for column end conditions, KL/r – slenderness ratio

Table 4.8 Comparisons of steel H-piles with no concrete encasements – HP10×57

Pile Length (L_b) (ft)	Area (in ²)	Moment of Inertia (in ⁴)	K	KL/r	Limit for Elastic Buckling	FE Results - Nonlinear Analysis (kips)	AISC Equations (kips)	FE Results - Linear Elastic Analysis (kips)	Euler Buckling Strength (kips)	Full Yield Strength (kips)
16	16.7	101	0.7	54.7	113.4	675	671	1588	1600	835
20	16.7	101	0.7	68.3	113.4	590	594	1021	1024	835
24	16.7	101	0.7	82.0	113.4	496	511	711	711	835
30	16.7	101	0.7	102.5	113.4	379	387	456	455	835
35	16.7	101	0.7	119.5	113.4	296	293	326	334	835
40	16.7	101	0.7	136.6	113.4	234	225	257	256	835

Table 4.9 Comparisons of steel H-piles with no concrete encasements – HP12×53

Pile Length (L_b) (ft)	Area (in ²)	Moment of Inertia (in ⁴)	K	KL/r	Limit for Elastic Buckling	FE Results - Nonlinear Analysis (kips)	AISC Equations (kips)	FE Results - Linear Elastic Analysis (kips)	Euler Buckling Strength (kips)	Full Yield Strength (kips)
19	15.5	127	0.7	55.8	113.4	616	613	1419	1427	775
25	15.5	127	0.7	73.4	113.4	516	520	825	824	775
30	15.5	127	0.7	88.0	113.4	496	438	574	572	775
35	15.5	127	0.7	102.7	113.4	350	358	423	421	775
40	15.5	127	0.7	117.4	113.4	284	282	324	322	775
45	15.5	127	0.7	132.1	113.4	232	223	256	254	775

Table 4.10 Comparisons of steel H-piles with no concrete encasements – HP14×73

Pile Length (L_b) (ft)	Area (in ²)	Moment of Inertia (in ⁴)	K	KL/r	Limit for Elastic Buckling	FE Results - Nonlinear Analysis (kips)	AISC Equations (kips)	FE Results - Linear Elastic Analysis (kips)	Euler Buckling Strength (kips)	Full Yield Strength (kips)
24	21.4	261	0.7	57.7	113.4	832	820	1836	1838	1070
30	21.4	261	0.7	72.2	113.4	721	718	1181	1176	1070
35	21.4	261	0.7	84.2	113.4	615	628	869	864	1070
40	21.4	261	0.7	96.2	113.4	529	538	667	662	1070
45	21.4	261	0.7	108.2	113.4	448	452	527	523	1070
50	21.4	261	0.7	120.3	113.4	377	371	427	423	1070
55	21.4	261	0.7	132.3	113.4	320	307	353	350	1070
60	21.4	261	0.7	144.3	113.4	273	258	297	294	1070

Table 4.11 Comparisons of steel H-piles with no concrete encasements – HP14×89

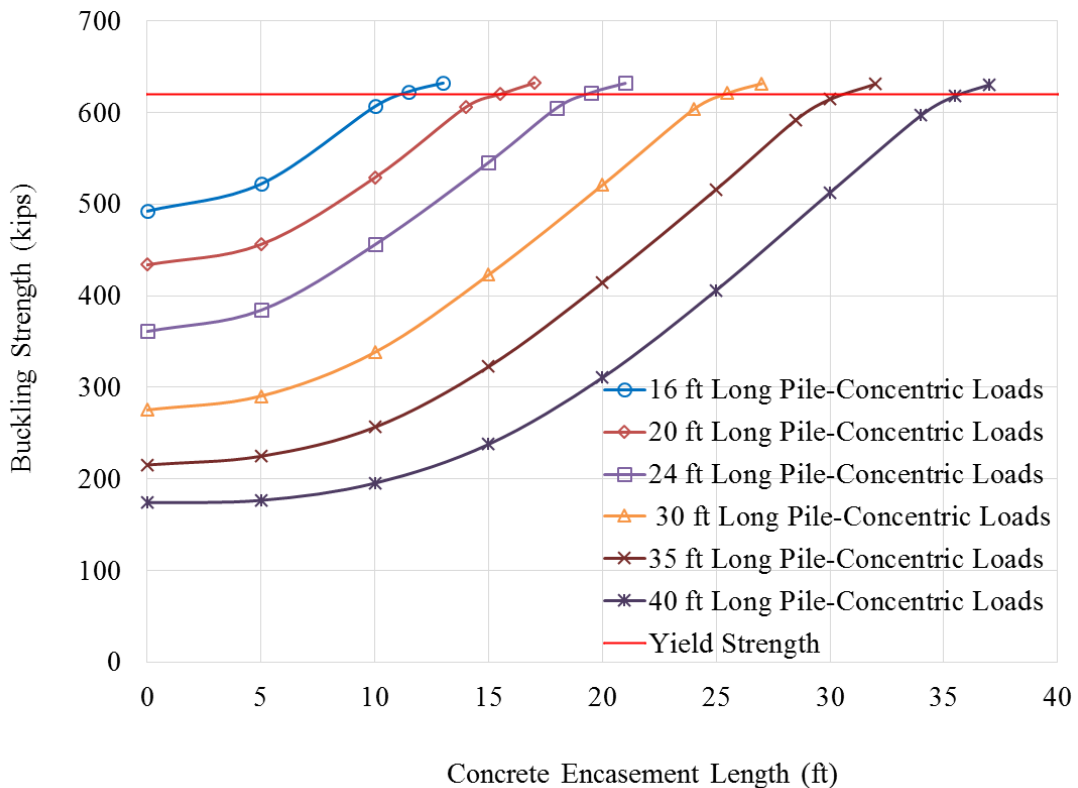
Pile Length (L_b) (ft)	Area (in ²)	Moment of Inertia (in ⁴)	K	KL/r	Limit for Elastic Buckling	FE Results - Nonlinear Analysis (kips)	AISC Equations (kips)	FE Results - Linear Elastic Analysis (kips)	Euler Buckling Strength (kips)	Full Yield Strength (kips)
24	26.1	326	0.7	57.0	113.4	1020	1029	2276	2296	1305
30	26.1	326	0.7	71.3	113.4	888	900	1463	1469	1305
35	26.1	326	0.7	83.2	113.4	758	787	1077	1079	1305
40	26.1	326	0.7	95.1	113.4	653	674	826	826	1305
45	26.1	326	0.7	107.0	113.4	555	565	653	653	1305
50	26.1	326	0.7	118.8	113.4	467	464	529	529	1305
55	26.1	326	0.7	130.7	113.4	396	383	438	437	1305
60	26.1	326	0.7	142.6	113.4	338	322	368	367	1305

Similar to the FE model validation process, the FE results in the linear elastic buckling analysis should be compared with those derived based on the Euler buckling equation; while the FE results in the nonlinear buckling analysis should be compared with those derived based on the AISC equations. As a further demonstration of the FE model validation process, the comparisons of FE results for the piles without concrete encasement with the Euler buckling strengths and the solutions from the AISC equations appear in Table 4.7 through Table 4.11. As shown in Table 4.7 through Table 4.11, the FE results in the linear elastic buckling analysis are very close to the Euler buckling strength; and the FE results in the nonlinear buckling analysis are very close to the solutions from the AISC equations.

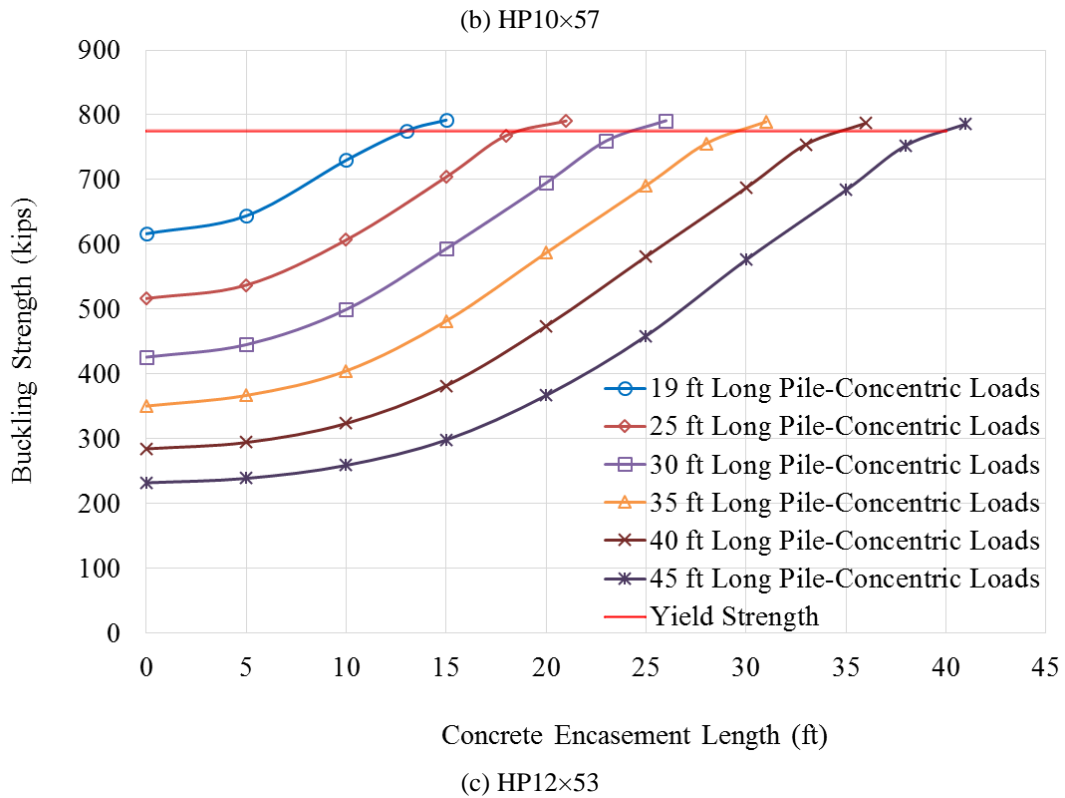
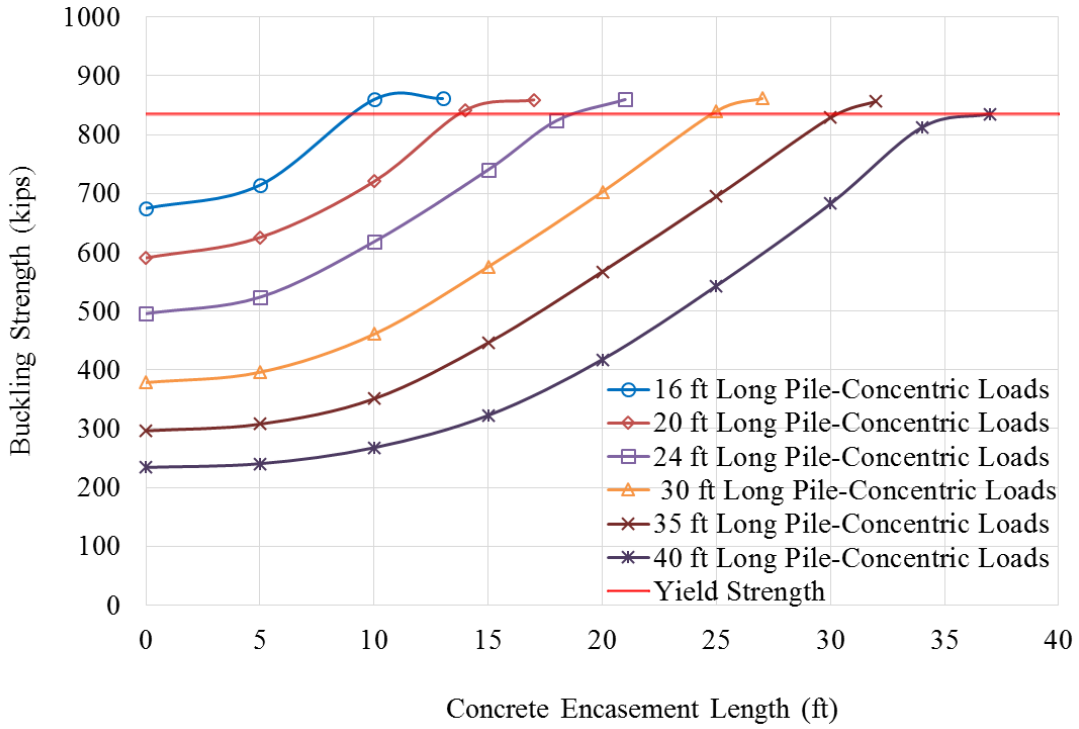
The full yield strength of the piles was also determined and appears in Table 4.7 through Table 4.11. As shown in Table 4.7 through Table 4.11, the full yield strength of the piles is the upper

bound of the buckling strength of the intermediate and long columns. The Euler buckling strength was higher than the full yield strength because the steel yield, geometric imperfection, and residual stress were not taken into account in the formula development. Accordingly, the adequacy of the FE models was further validated by comparing the FE results with those derived from the verified resources.

Taking into account the number of pile lengths (L_b) and the amount of associated concrete encasement lengths shown in Table 4.2 through Table 4.6, 242 FE models were established based on the FE modeling techniques introduced in Chapter 3. After the concentric load was applied until buckling failure occurred, the buckling strength of the steel H-piles was then determined from the FE models. The relationship between buckling strength of the steel H-piles for the cross-sections of HP10×42, HP10×57, HP12×43, HP14×73, and HP14×89 and concrete encasement length are as shown in Figure 4.3(a), Figure 4.3(b), Figure 4.3(c), Figure 4.3(d), and Figure 4.3(e), respectively.



(a) HP10×42



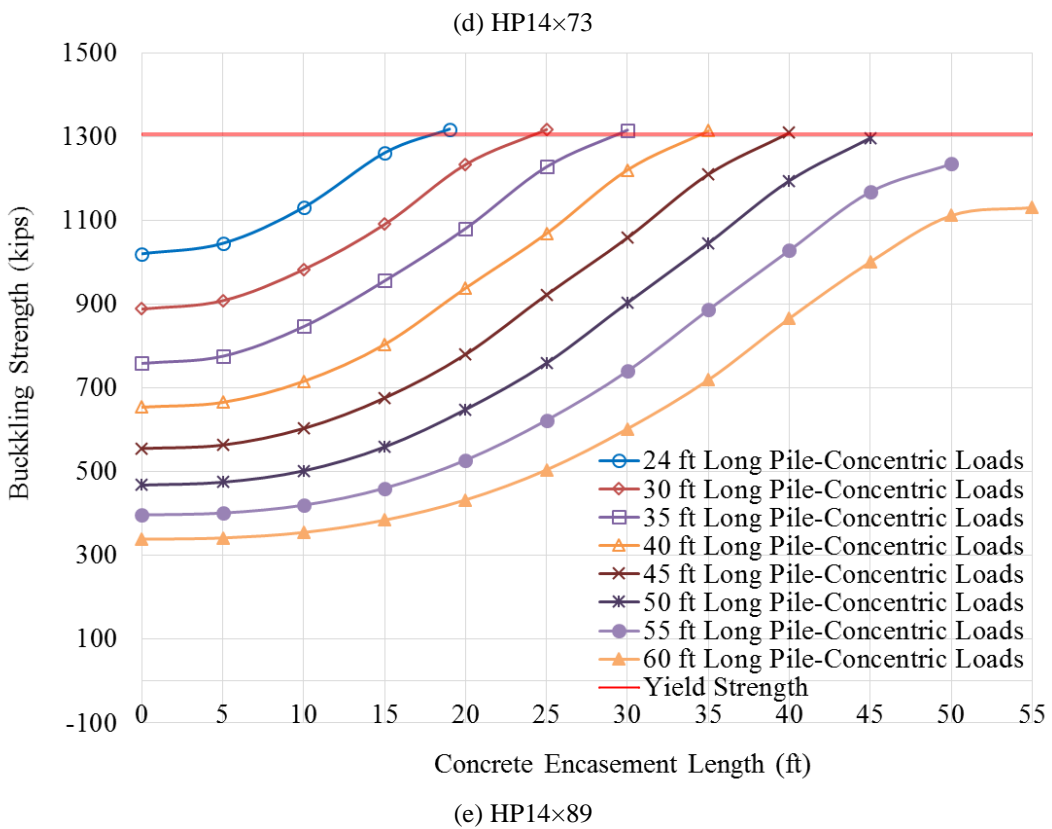
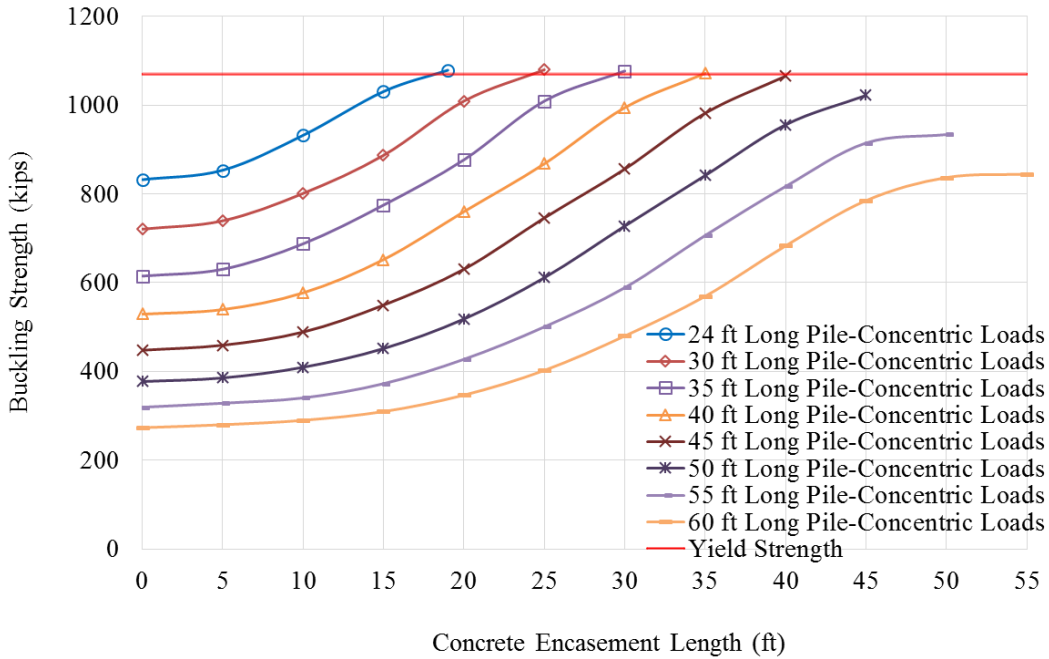


Figure 4.3 Buckling strength of steel H-piles with different concrete encasement lengths under concentric loads

Figure 4.3 indicates that the buckling strength of the steel H-piles increases along with the increase in concrete encasement length. The maximum buckling strength could be slightly larger

than the full yield strength because the von Mises yield criteria were utilized in the FE models. However, to be conservative and consistent with the codified specifications, the maximum buckling strength should be taken as no more than the full yield strength. As shown in Figure 4.3, the solid line without markers in the plot for each pile section indicates the full yield strength for that pile section.

4.3 Pile Bents with Eccentric Loads

As mentioned previously, it is commonly assumed that the pile bents have a load eccentricity of 2 in. for both axes for both design and load ratings. The selected piles with the unbraced pile length and the concrete encasement length shown in Table 4.2 through Table 4.6 were further utilized to study the cases with eccentric loads.

For the steel H-piles without concrete encasement, per the AASHTO LRFD Bridge Design Specifications (AASHTO 2015), the strength of the columns under eccentric loads (P_u) should be estimated by the following equations:

$$\frac{P_u}{P_r} + 8 \left(\frac{M_{ux}}{M_{rx}} + \frac{M_{uy}}{M_{ry}} \right) \leq 1.0 \quad \text{for } \frac{P_u}{P_r} \geq 0.2 \quad (9)$$

$$\frac{P_u}{2P_r} + \left(\frac{M_{ux}}{M_{rx}} + \frac{M_{uy}}{M_{ry}} \right) \leq 1.0 \quad \text{for } \frac{P_u}{P_r} < 0.2 \quad (10)$$

The maximum compressive load that can be applied to a pile under the eccentric loading condition (i.e., pile buckling strength under concentric loads), and P_r , can be derived by Eq. (1). P_u is the maximum compressive load that can be applied to a pile under the eccentric loading condition and must be determined from the pile strength estimation equations [Eq. (1) and Eq. (2) without a less than 1 resistance factor]. Concurrent moments, M_{ux} and M_{uy} can be determined by multiplying P_u by the 2-in. eccentricity about the two axes. The nominal flexural resistance for flexure about the weak axis (M_{ry}) should be taken as:

$$\text{If } \lambda_f \leq \lambda_{pf}, \quad M_{ry} = M_p \quad (11)$$

$$\text{If } \lambda_{pf} < \lambda_f \leq \lambda_{rf}, \quad M_{ry} = \left[1 - \left(1 - \frac{S_y}{Z_y} \right) \left(\frac{\lambda_f - \lambda_{pf}}{0.45 \sqrt{\frac{E}{F_y}}} \right) \right] \quad (12)$$

where

λ_f = slenderness ratio for the flange can be expressed as:

$$\lambda_f = \frac{b_f}{2t_f} \quad (13)$$

λ_{pf} = slenderness ratio for the flange can be expressed as:

$$\lambda_{pf} = 0.38 \sqrt{\frac{E}{F_{yf}}} \quad (14)$$

λ_{pf} = limiting slenderness ratio for a non-compact flange can be expressed as:

$$\lambda_{pf} = 0.83 \sqrt{\frac{E}{F_{yf}}} \quad (15)$$

where

F_{yf} = specified minimum yield strength of the flange

M_p = plastic moment about the weak axis

S_y = elastic section modulus about weak axis

Z_y = plastic section modulus about the weak axis

The nominal flexural resistance for flexure about the strong axis (M_{rx}) should be taken as (without resistance factors but with considering local buckling per AISC):

$$M_{rx} = F_{nc} \cdot S_x \quad (16)$$

$$\text{If } L_b \leq L_p, \quad F_{nc} = F_{yc} \quad (17)$$

$$\text{If } L_p < L_b \leq L_r, \quad F_{nc} = C_b \left[1 - \left(1 - \frac{F_{yr}}{F_{yc}} \right) \left(\frac{L_b - L_p}{L_r - L_p} \right) \right] F_{yc} \leq F_{yc} \quad (18)$$

$$\text{If } L_b > L_r, \quad F_{nc} = F_{cr} \leq F_{yc} \quad (19)$$

where

F_{nc} = nominal flexural resistance of the flange

F_{yc} = yield strength of a compression flange

L_b = unbraced length

L_p = limiting unbraced length to achieve the nominal flexural resistance under uniform bending can be expressed as:

$$L_p = 1.0 r_t \sqrt{\frac{E}{F_{yc}}} \quad (20)$$

L_r = limiting unbraced length to achieve the onset of nominal yielding in either flange under uniform bending with consideration of compression flange residual stress effects can be expressed as:

$$L_r = \pi r_t \sqrt{\frac{E}{F_{yr}}} \quad (21)$$

where

C_b = moment gradient modifier, 1.0; $F_{yr} = 0.7F_{yc}$

F_{cr} = elastic lateral torsional buckling stress can be expressed as:

$$F_{cr} = \frac{C_b \pi^2 E}{\left(\frac{L_b}{r_t} \right)^2} \quad (22)$$

r_t = effective radius of gyration for lateral torsional buckling can be expressed as:

$$r_t = \frac{b_{fc}}{\sqrt{12 \left(1 + \frac{1}{3} \frac{D_c t_w}{b_{fc} t_{fc}} \right)}} \quad (23)$$

where

D_c = depth of the web in compression in the elastic range

t_w = thickness of the web

b_{fc} = width of the flange

t_{fc} = thickness of the flange

Based on Equations (9) through (23), for pile section HP10×42, the pile buckling strength under eccentric loads (P_u), concurrent moments (M_{ux} and M_{uy}), the pile buckling strength under concentric loads (P_r), the nominal flexural resistance for flexure about the weak axis (M_{ry}), and the nominal flexural resistance for flexure about the strong axis (M_{rx}) were calculated and are summarized in Table 4.12 and Table 4.13. Note that the various values in these tables follow the calculations summarized by Equations 9–23.

Likewise, based on Equations (9) through (23), for pile section HP10×57, combined axial compression and flexure calculation results are summarized in Table 4.14 and Table 4.15; for pile section HP12×53, combined axial compression and flexure calculation results are summarized in Table 4.16 and Table 4.17; for pile section HP14×73, combined axial compression and flexure calculation results are summarized in Table 4.18 and Table 4.19; and for pile section HP14×89, combined axial compression and flexure calculation results are summarized in Table 4.20 and Table 4.21.

Additionally, the pile buckling strength derived from the FE models of the steel H-piles without concrete encasement was also included in Table 4.12 through Table 4.21. Reviewing the comparisons between pile strengths derived from the AISC equations and FE results, the AISC equations fairly regularly underestimate the pile buckling strength under eccentric loads. This finding is consistent with the specifications included in the AISC Steel Construction Manual (AISC 2017) with the intent of using conservative estimates to ensure a sufficient safety margin.

The estimated differences between the AISC equations and FE results are included in Table 4.12 through Table 4.21. To achieve the same safety margin levels through conservative estimates for steel H-piles with concrete encasements, the estimation differences were further utilized for the development of the pile assessment tool, which is covered in the next section. Note that no resistance factors have been utilized to minimize confusion with AISC-type calculations.

Table 4.12 Combined axial compression and flexure calculations including flexural resistance about strong axis – HP10×42

Pile Length (ft)	Pile Length (in.)	Area _x (in. ²)	Moment of Inertia _x (in. ⁴)	S _x (in ³)	K _x	K _x L _b /r _x	Limit _x	r _t (in.)	L _r (in.)	L _p (in.)	F _{nc} (ksi)	P _{cr} (kips)	δ _b	M _{rx} (kip-ft)	P _{cx} (kips)	M _{cx} (kip-ft)	P _r /P _c	PR	P _r per AISC Equations (kips)	FE Results - Nonlinear (kips)	Estimation Difference (kips)
16	192	12.4	210	43.4	1	32.5	113.4	2.7	246.5	65.6	39.5	3351	1.06	33.6	573	142.9	0.33	1.004	190	212	22
20	240	12.4	210	43.4	1	40.7	113.4	2.7	246.5	65.6	35.5	2145	1.09	30.8	549	128.5	0.31	1.003	170	208	38
24	288	12.4	210	43.4	1	48.8	113.4	2.7	246.5	65.6	25.6	1489	1.11	26.6	520	92.7	0.28	1.005	144	198	54
30	360	12.4	210	43.4	1	61.0	113.4	2.7	246.5	65.6	16.4	953	1.13	20.7	471	59.3	0.23	1.006	110	174	64
35	420	12.4	210	43.4	1	71.2	113.4	2.7	246.5	65.6	12.1	700	1.16	19.0	614	43.6	0.16	1.008	98	145	47
40	480	12.4	210	43.4	1	81.4	113.4	2.7	246.5	65.6	9.2	536	1.18	15.7	470	33.4	0.17	1.009	80	122	42

PR – Performance ratio

Table 4.13 Combined axial compression and flexure calculations including flexural resistance about weak axis of the piles under eccentric loads – HP10×42

Pile Length (ft)	Pile Length (in.)	Area _y (in. ²)	Moment of Inertia _y (in. ⁴)	S _y (in ³)	K _y	K _y L _b /r _y	Limit _y	λ _t	λ _{rf}	λ _{pf}	Z _y (in ³)	P _{cr} (kips)	δ _b	M _{ry} (kip-ft)	P _{cy} (kips)	M _{cy} (kip-ft)
16	192	12.4	71.7	14.2	1	55.9	113.4	12.0	9.2	20.0	21.8	1136	1.20	38.0	493	82.4
20	240	12.4	71.7	14.2	1	69.9	113.4	12.0	9.2	20.0	21.8	727	1.31	37.0	434	82.4
24	288	12.4	71.7	14.2	1	83.8	113.4	12.0	9.2	20.0	21.8	504.9	1.40	33.6	371	82.4
30	360	12.4	71.7	14.2	1	104.8	113.4	12.0	9.2	20.0	21.8	323	1.52	27.8	278	82.4
35	420	12.4	71.7	14.2	1	122.3	113.4	12.0	9.2	20.0	21.8	237	1.70	27.8	208	82.4
40	480	12.4	71.7	14.2	1	139.7	113.4	12.0	9.2	20.0	21.8	182	1.79	23.8	159	82.4

Table 4.14 Combined axial compression and flexure calculations including flexural resistance about strong axis of the piles under eccentric loads – HP10×57

Pile Length (ft)	Pile Length (in.)	Area _x (in. ²)	Moment of Inertia _x (in. ⁴)	S _x (in. ³)	K _x	K _x L _b /r _x	Limit _x	r _t (in.)	L _r (in.)	L _p (in.)	F _{nc} (ksi)	P _{cr} (kips)	δ _b	M _{rx} (kip-ft)	P _{cx} (kips)	M _{cx} (kip-ft)	P _r /P _c	PR	P _r per AISC Equations (kips)	FE Results - Nonlinear (kips)	Estimation Difference (kips)
16	192	16.7	294	59	0.7	32.0	113.4	2.75	248.9	66.3	39.7	4659	1.06	47.8	775	194.4	0.35	1.002	270	333.8	64
20	240	16.7	294	59	0.7	40.0	113.4	2.75	248.9	66.3	35.7	2981	1.09	43.9	743	175.1	0.33	1.002	242	323.8	82
24	288	16.7	294	59	0.7	48.0	113.4	2.75	248.9	66.3	26.1	2070	1.11	37.9	705	128.1	0.29	1.002	205	301.5	96
30	360	16.7	294	59	0.7	60.1	113.4	2.75	248.9	66.3	16.7	1325	1.13	29.5	641	82.0	0.24	1.001	156	241.9	86
35	420	16.7	294	59	0.7	70.1	113.4	2.75	248.9	66.3	12.3	974	1.15	23.7	583	60.2	0.21	1.004	124	201.4	77
40	480	16.7	294	59	0.7	80.1	113.4	2.75	248.9	66.3	9.4	745	1.15	19.0	522	46.1	0.19	0.997	99	169.2	70

PR – Performance ratio

Table 4.15 Combined axial compression and flexure calculations including flexural resistance about weak axis of the piles under eccentric loads – HP10×57

Pile Length (ft)	Pile Length (in.)	Area _y (in. ²)	Moment of Inertia _y (in. ⁴)	S _y (in. ³)	K _y	K _y L _b /r _y	Limit _y	λ _t	λ _{rt}	λ _{pr}	Z _y (in. ³)	P _{cr} (kips)	δ _b	M _{ry} (kip-ft)	P _{cy} (kips)	M _{cy} (kip-ft)
16	192	16.7	101	20	0.7	54.7	113.4	9.0	9.2	20.0	30.3	1600	1.20	54.1	671	126.3
20	240	16.7	101	20	0.7	68.3	113.4	9.0	9.2	20.0	30.3	1024	1.31	52.8	594	126.3
24	288	16.7	101	20	0.7	82.0	113.4	9.0	9.2	20.0	30.3	711.3	1.40	48.0	511	126.3
30	360	16.7	101	20	0.7	102.5	113.4	9.0	9.2	20.0	30.3	455	1.52	39.6	387	126.3
35	420	16.7	101	20	0.7	119.5	113.4	9.0	9.2	20.0	30.3	334	1.59	32.8	293	126.3
40	480	16.7	101	20	0.7	136.6	113.4	9.0	9.2	20.0	30.3	256	1.63	26.9	225	126.3

Table 4.16 Combined axial compression and flexure calculations including flexural resistance about strong axis of the piles under eccentric loads – HP12×53

Pile Length (ft)	Pile Length (in.)	Area _x (in. ²)	Moment of Inertia _x (in. ⁴)	S _x (in. ³)	K _x	K _x L _b /r _x	Limit _x	r _t (in.)	L _r (in.)	L _p (in.)	F _{nc} (ksi)	P _{cr} (kips)	δ _b	M _{rx} (kip-ft)	P _{cx} (kips)	M _{cx} (kip-ft)	P _r /P _c	PR	P _r per AISC Equations (kips)	FE Results - Nonlinear (kips)	Estimation Difference (kips)
19	228	15.5	393	66.7	0.7	31.7	113.4	3.2	291.9	77.7	39.5	4416	1.06	44.5	720	219.4	0.35	1.001	252	356.4	104
25	300	15.5	393	66.7	0.7	41.7	113.4	3.2	291.9	77.7	33.1	2551	1.09	39.5	682	184.2	0.32	1.003	217	319.3	102
30	360	15.5	393	66.7	0.7	50.0	113.4	3.2	291.9	77.7	23.0	1771	1.11	33.6	645	127.9	0.28	1.002	181	272.3	91
35	420	15.5	393	66.7	0.7	58.4	113.4	3.2	291.9	77.7	16.9	1301	1.13	28.3	604	94.0	0.25	1.000	150	231.3	81
40	480	15.5	393	66.7	0.7	66.7	113.4	3.2	291.9	77.7	12.9	996	1.14	23.6	560	71.9	0.22	1.003	124	196.2	72
45	540	15.5	393	66.7	0.7	75.1	113.4	3.2	291.9	77.7	10.2	787	1.15	19.8	513	56.8	0.20	1.004	103	168.4	65

PR – Performance ratio

Table 4.17 Combined axial compression and flexure calculations including flexural resistance about weak axis of the piles under eccentric loads – HP12×53

Pile Length (ft)	Pile Length (in.)	Area _y (in. ²)	Moment of Inertia _y (in. ⁴)	S _y (in. ³)	K _y	K _y L _b /r _y	Limit _y	λ _r	λ _{rf}	λ _{pf}	Z _y (in. ³)	P _{cr} (kips)	δ _b	M _{ry} (kip-ft)	P _{cy} (kips)	M _{cy} (kip-ft)
19	228	15.5	127	21.1	0.7	55.8	113.4	13.8	9.2	20.0	30.3	1427	1.21	51.0	617	109.8
25	300	15.5	127	21.1	0.7	73.4	113.4	13.8	9.2	20.0	30.3	824	1.36	49.1	523	109.8
30	360	15.5	127	21.1	0.7	88.0	113.4	13.8	9.2	20.0	30.3	572.4	1.46	44.1	440	109.8
35	420	15.5	127	21.1	0.7	102.7	113.4	13.8	9.2	20.0	30.3	421	1.55	38.9	358	109.8
40	480	15.5	127	21.1	0.7	117.4	113.4	13.8	9.2	20.0	30.3	322	1.63	33.6	282	109.8
45	540	15.5	127	21.1	0.7	132.1	113.4	13.8	9.2	20.0	30.3	254	1.68	28.8	223	109.8

Table 4.18 Combined axial compression and flexure calculations including flexural resistance about strong axis of the piles under eccentric loads – HP14×73

Pile Length (ft)	Pile Length (in.)	Area _x (in. ²)	Moment of Inertia _x (in. ⁴)	S _x (in. ³)	K _x	K _x L _b /r _x	Limit _x	r _t (in.)	L _r (in.)	L _p (in.)	F _{nc} (ksi)	P _{cr} (kips)	δ _b	M _{rx} (kip-ft)	P _{cx} (kips)	M _{cx} (kip-ft)	P _r /P _c	PR	P _r per AISC Equations (kips)	FE Results - Nonlinear (kips)	Estimation Difference (kips)
24	288	21.4	729	107	0.7	34.5	113.4	3.9	356.4	94.9	38.6	5134	1.08	67.4	954	344.0	0.39	1.001	375	535	160
30	360	21.4	729	107	0.7	43.2	113.4	3.9	356.4	94.9	34.3	3286	1.11	61.3	910	305.8	0.36	1.000	331	530	199
35	420	21.4	729	107	0.7	50.4	113.4	3.9	356.4	94.9	25.2	2414	1.13	53.9	868	224.7	0.33	1.000	285	414	129
40	480	21.4	729	107	0.7	57.6	113.4	3.9	356.4	94.9	19.3	1848	1.15	47.1	821	172.0	0.30	1.003	245	361	116
45	540	21.4	729	107	0.7	64.8	113.4	3.9	356.4	94.9	15.2	1460	1.17	40.7	771	135.9	0.27	1.001	209	315	106
50	600	21.4	729	107	0.7	72.0	113.4	3.9	356.4	94.9	12.3	1183	1.18	34.9	719	110.1	0.25	1.001	178	276	98
55	660	21.4	729	107	0.7	79.2	113.4	3.9	356.4	94.9	10.2	978	1.18	29.8	666	91.0	0.23	1.002	151	243	92
60	720	21.4	729	107	0.7	86.4	113.4	3.9	356.4	94.9	8.6	821	1.18	25.0	612	76.5	0.21	1.002	127	215	88

PR – Performance ratio

Table 4.19 Combined axial compression and flexure calculations including flexural resistance about weak axis of the piles under eccentric loads – HP14×73

Pile Length (ft)	Pile Length (in.)	Area _y (in. ²)	Moment of Inertia _y (in. ⁴)	S _y (in. ³)	K _y	K _y L _b /r _y	Limit _y	λ _t	λ _{rt}	λ _{pf}	Z _y (in. ³)	P _{cr} (kips)	δ _b	M _{ry} (kip-ft)	P _{cy} (kips)	M _{cy} (kip-ft)
24	288	21.4	261	35.8	0.7	57.7	113.4	14.5	9.2	20.0	54.6	1838	1.26	78.5	820	189.2
30	360	21.4	261	35.8	0.7	72.2	113.4	14.5	9.2	20.0	54.6	1176	1.39	76.8	718	189.2
35	420	21.4	261	35.8	0.7	84.2	113.4	14.5	9.2	20.0	54.6	864.3	1.49	70.9	628	189.2
40	480	21.4	261	35.8	0.7	96.2	113.4	14.5	9.2	20.0	54.6	662	1.59	64.8	538	189.2
45	540	21.4	261	35.8	0.7	108.2	113.4	14.5	9.2	20.0	54.6	523	1.67	58.0	452	189.2
50	600	21.4	261	35.8	0.7	120.3	113.4	14.5	9.2	20.0	54.6	423	1.73	51.2	372	189.2
55	660	21.4	261	35.8	0.7	132.3	113.4	14.5	9.2	20.0	54.6	350	1.76	44.3	300	189.2
60	720	21.4	261	35.8	0.7	144.3	113.4	14.5	9.2	20.0	54.6	294	1.76	37.3	237	189.2

Table 4.20 Combined axial compression and flexure calculations including flexural resistance about strong axis of the piles under eccentric loads – HP14×89

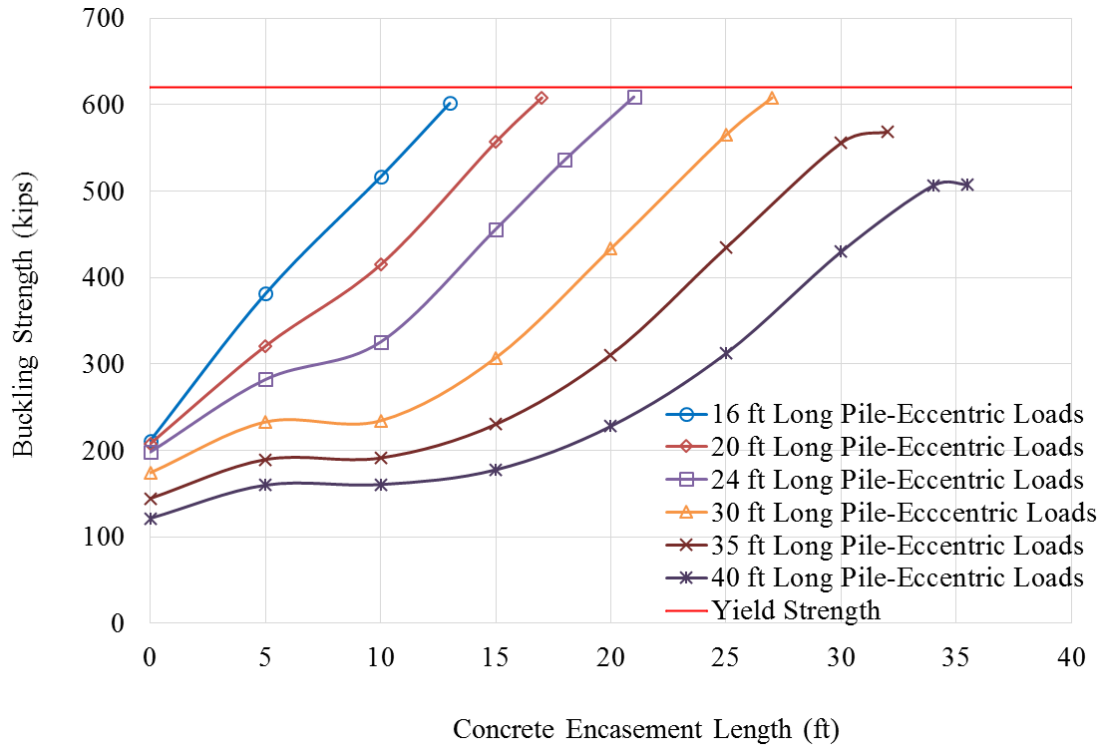
Pile Length (ft)	Pile Length (in.)	Area _x (in. ²)	Moment of Inertia _x (in. ⁴)	S _x (in. ³)	K _x	K _x L _b /r _x	Limit _x	r _t (in.)	L _r (in.)	L _p (in.)	F _{nc} (ksi)	P _{cr} (kips)	δ _b	M _{rx} (kip-ft)	P _{cx} (kips)	M _{cx} (kip-ft)	P _r /P _c	PR	P _r per AISC Equations (kips)	FE Results - Nonlinear (kips)	Estimation Difference (kips)
24	288	26.1	904	131	0.7	34.3	113.4	3.97	359	95.6	39.0	6366	1.08	87.1	1198	426.2	0.40	1.004	483	679	196
30	360	26.1	904	131	0.7	42.8	113.4	3.97	359	95.6	34.8	4074	1.12	79.3	1141	380.0	0.37	1.005	426	588	162
35	420	26.1	904	131	0.7	50.0	113.4	3.97	359	95.6	25.6	2993	1.14	69.5	1087	279.2	0.34	1.006	366	513	147
40	480	26.1	904	131	0.7	57.1	113.4	3.97	359	95.6	19.6	2292	1.16	60.4	1028	213.7	0.30	1.006	313	448	135
45	540	26.1	904	131	0.7	64.2	113.4	3.97	359	95.6	15.5	1811	1.17	52.2	965	168.9	0.28	1.007	267	390	123
50	600	26.1	904	131	0.7	71.4	113.4	3.97	359	95.6	12.5	1467	1.18	44.5	899	136.8	0.25	1.004	226	344	118
55	660	26.1	904	131	0.7	78.5	113.4	3.97	359	95.6	10.4	1212	1.19	38.3	832	113.1	0.23	1.003	193	299	106
60	720	26.1	904	131	0.7	85.6	113.4	3.97	359	95.6	8.7	1019	1.20	33.3	763	95.0	0.22	1.006	167	265	98

PR – Performance ratio

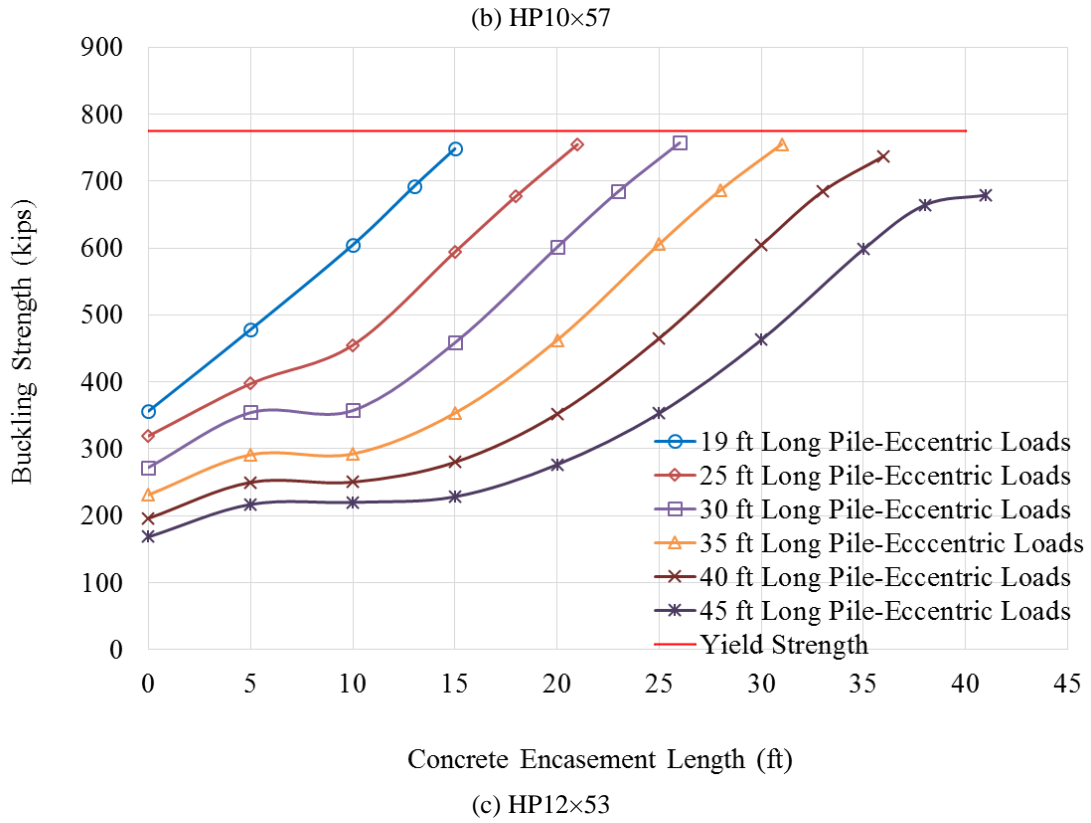
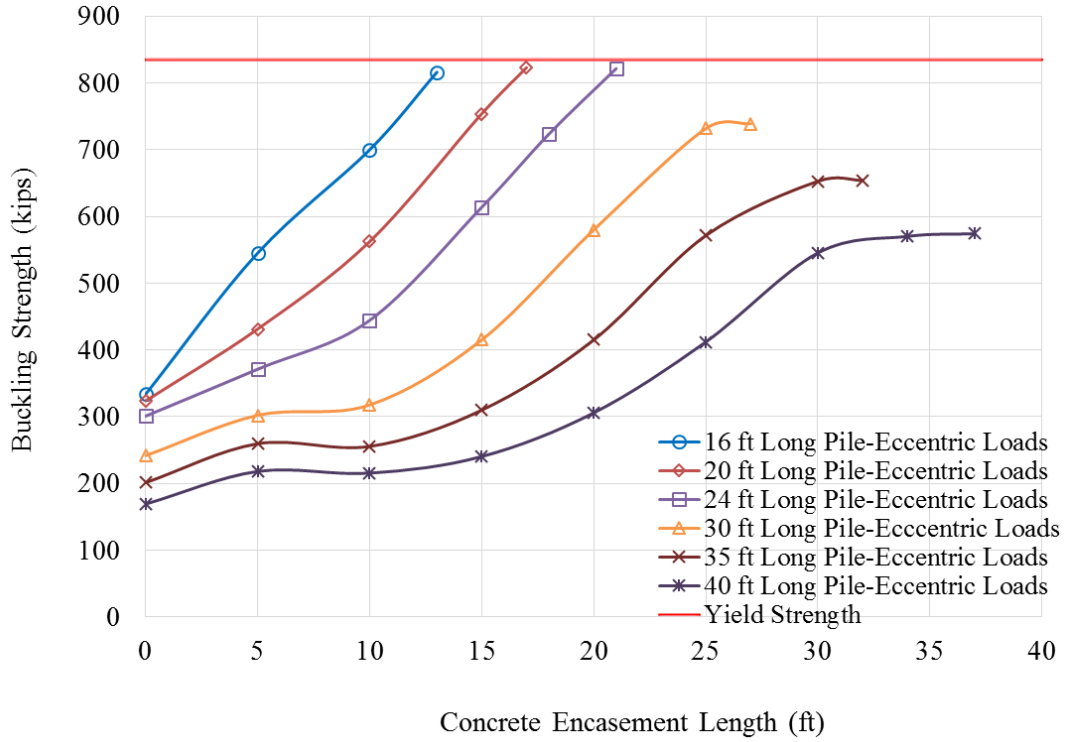
Table 4.21 Combined axial compression and flexure calculations including flexural resistance about weak axis of the piles under eccentric loads – HP14×89

Pile Length (ft)	Pile Length (in.)	Area _y (in. ²)	Moment of Inertia _y (in. ⁴)	S _y (in. ³)	K _y	K _y L _b /r _y	Limit _y	λ _t	λ _{tr}	λ _{pf}	Z _y (in. ³)	P _{cr} (kips)	δ _b	M _{ry} (kip-ft)	P _{cy} (kips)	M _{cy} (kip-ft)
24	288	26.1	326	44.3	0.7	57.0	113.4	12.0	9.2	20.0	67.7	2296	1.27	101.9	1029	256.9
30	360	26.1	326	44.3	0.7	71.3	113.4	12.0	9.2	20.0	67.7	1469	1.41	100.0	900	256.9
35	420	26.1	326	44.3	0.7	83.2	113.4	12.0	9.2	20.0	67.7	1079	1.51	92.3	787	256.9
40	480	26.1	326	44.3	0.7	95.1	113.4	12.0	9.2	20.0	67.7	826	1.61	84.0	674	256.9
45	540	26.1	326	44.3	0.7	107.0	113.4	12.0	9.2	20.0	67.7	653	1.69	75.3	565	256.9
50	600	26.1	326	44.3	0.7	118.8	113.4	12.0	9.2	20.0	67.7	529	1.75	65.8	464	256.9
55	660	26.1	326	44.3	0.7	130.7	113.4	12.0	9.2	20.0	67.7	437	1.79	57.6	383	256.9
60	720	26.1	326	44.3	0.7	142.6	113.4	12.0	9.2	20.0	67.7	367	1.83	51.0	322	256.9

To estimate the pile buckling strength under eccentric loads, taking into account the number of pile lengths (L_b) and the amount of associated concrete encasement lengths as shown in Table 4.2 through Table 4.6, 242 FE models were established based on the FE modeling techniques introduced in Chapter 3. After the eccentric load was applied and until buckling failure occurred, the buckling strength of the steel H-piles was derived from the FE models. The changes of the buckling strength of the steel H-piles for the cross-sections of HP10×42, HP10×57, HP12×53, HP14×73, and HP14×89 were plotted as shown in Figure 4.4(a), Figure 4.4(b), Figure 4.4(c), Figure 4.4(d), and Figure 4.4(e), respectively.



(a) HP10×42



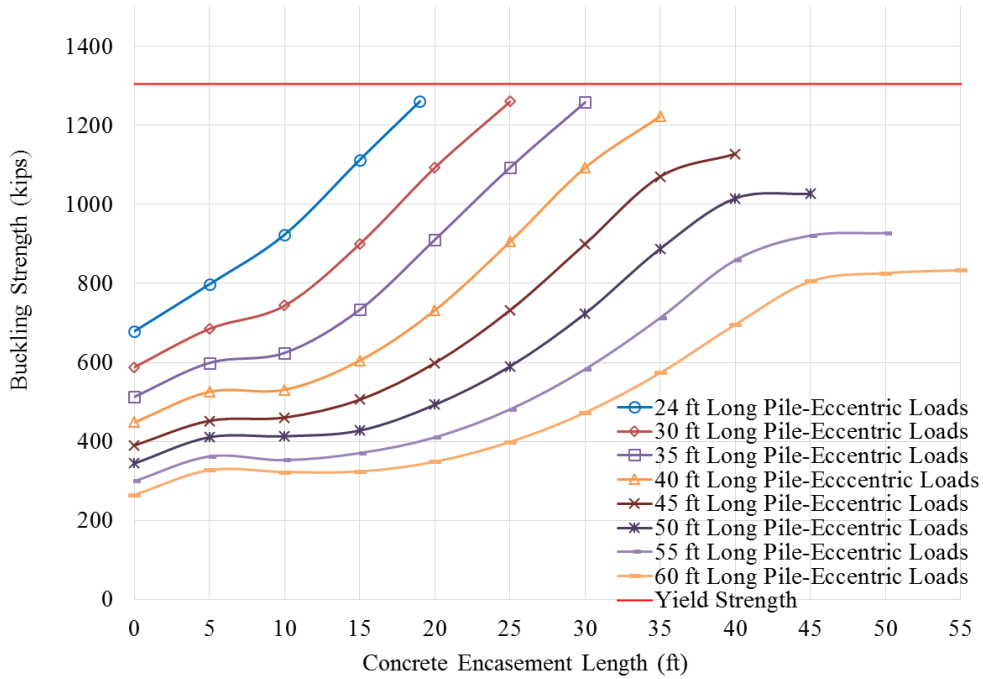
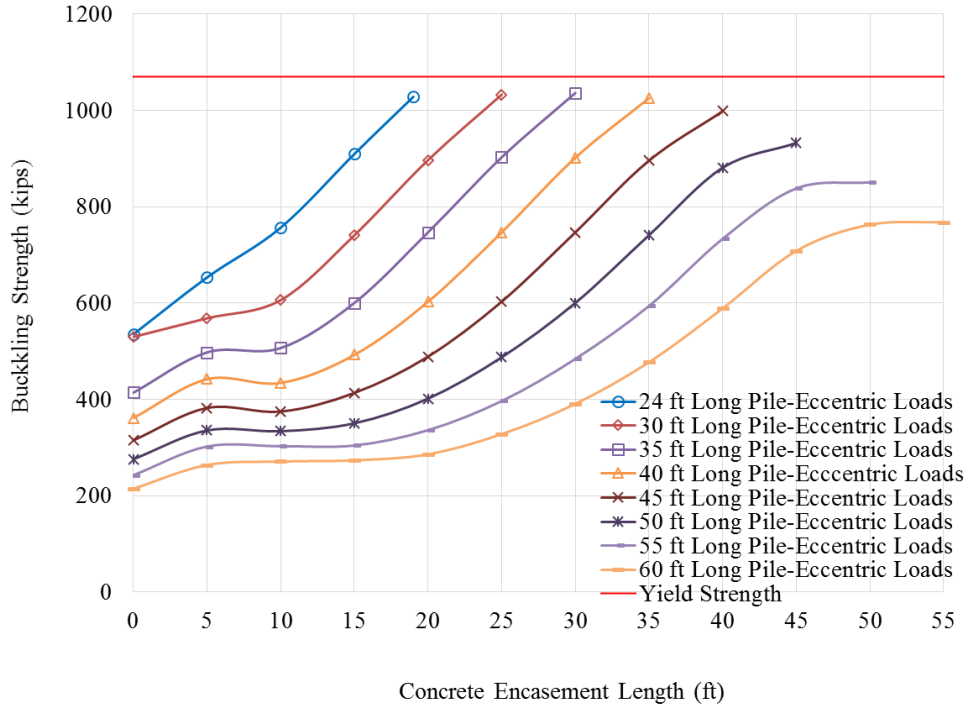


Figure 4.4 Buckling strength of steel H-piles with different concrete encasement lengths under eccentric loads

Figure 4.4 indicates that the buckling strength of the steel H-piles increases along with the increase in concrete encasement length. The maximum buckling strength is generally smaller

than the full yield strength because of the load eccentricity. As shown in Figure 4.4, the solid line without markers in the plot for each pile section indicates the full yield strength for that pile section.

4.4 Pile Assessment Tool Development

The stiffness contribution of concrete encasement is not taken into account by the AISC Steel Construction Manual (AISC 2017) and AASHTO LRFD specifications (AASHTO 2015) for estimating the buckling strength of steel H-piles with concrete encasement. The goal of this research is to develop a pile assessment tool to quickly calculate the buckling strength of steel H-piles with concrete encasement.

As shown in Figure 4.5, the predictions made for the buckling strength of steel H-piles with concentric loads or no concrete encasement that use the AISC equations are in good agreement with the FE results. However, as shown in Figure 4.6, predictions made for the buckling strength of steel H-piles with eccentric loads or no concrete encasement are underestimated when using the AISC equations compared to the FE results.

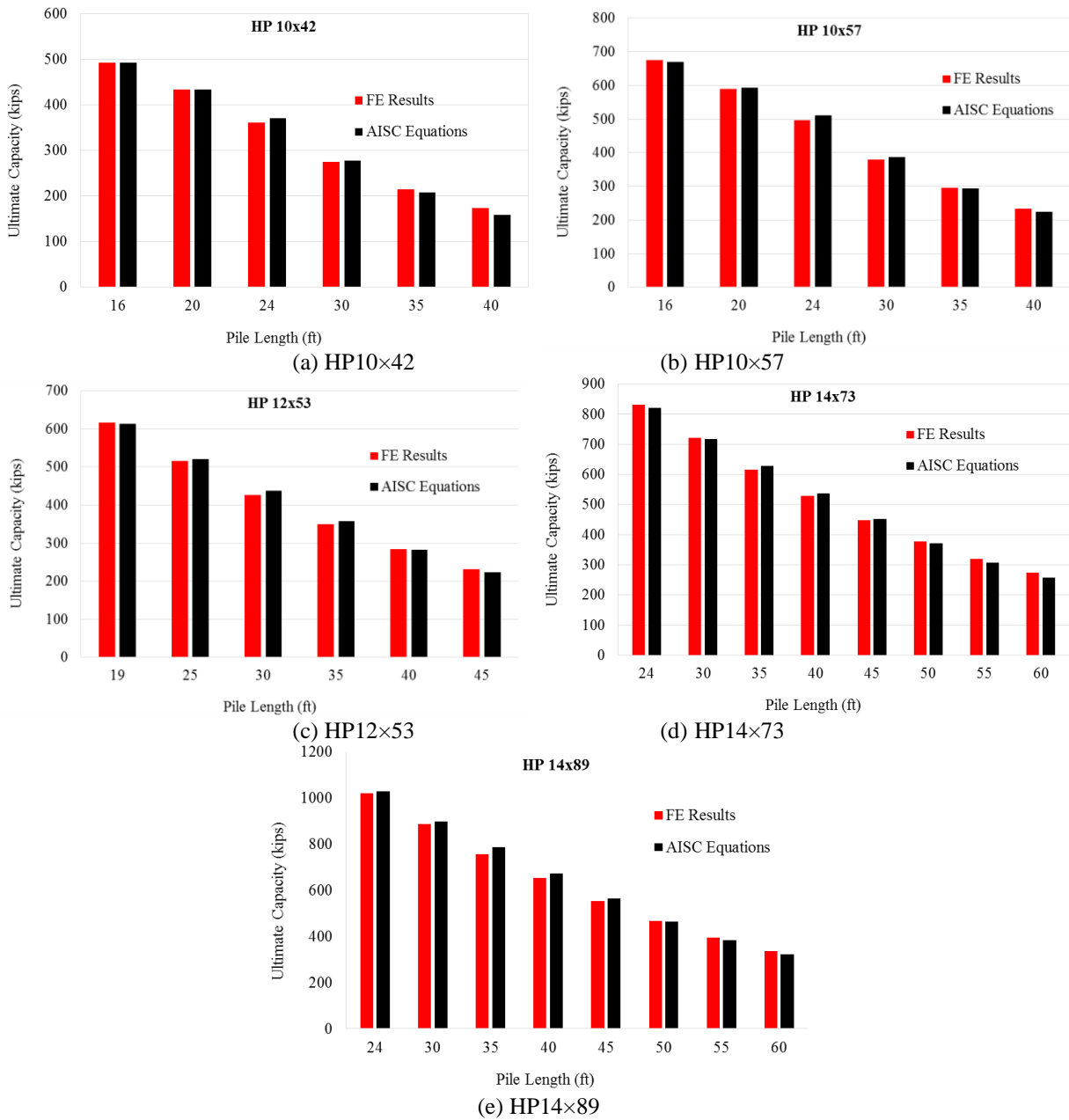


Figure 4.5 Comparisons between the pile strengths derived from the AISC equations and FE results – concentric loads/no concrete encasement

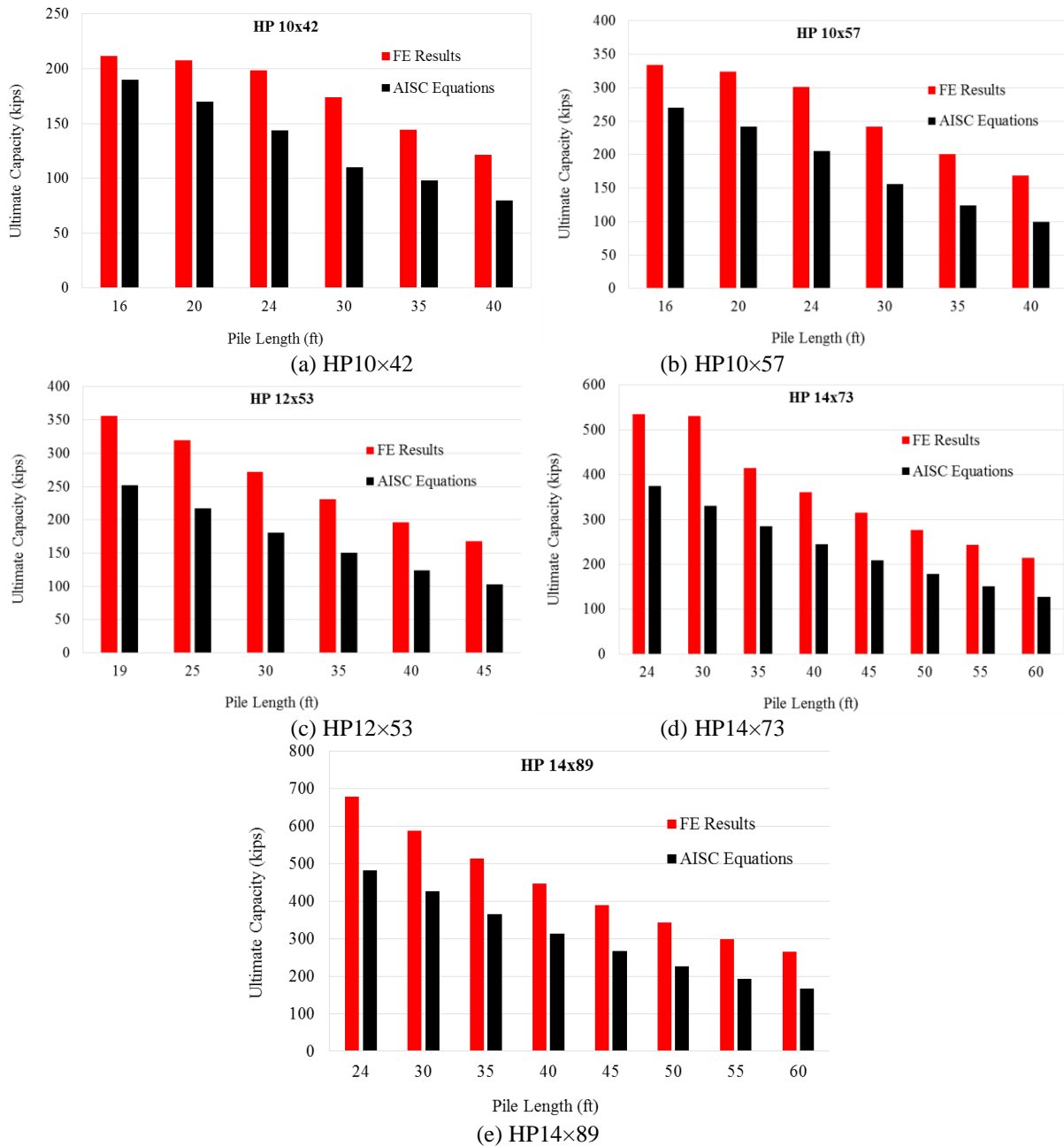
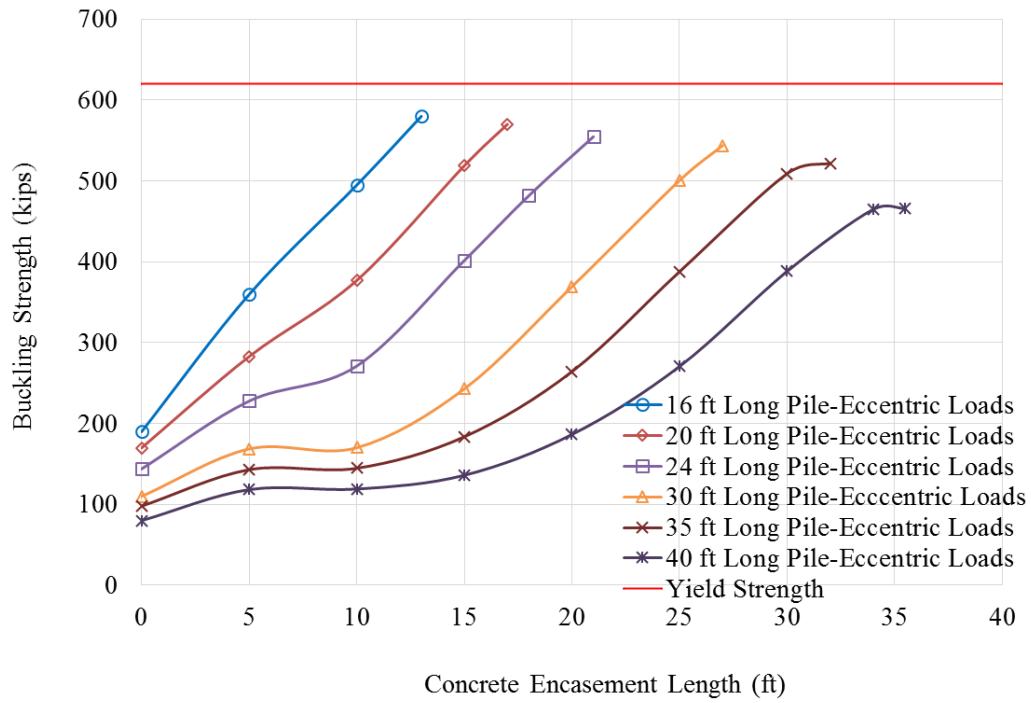
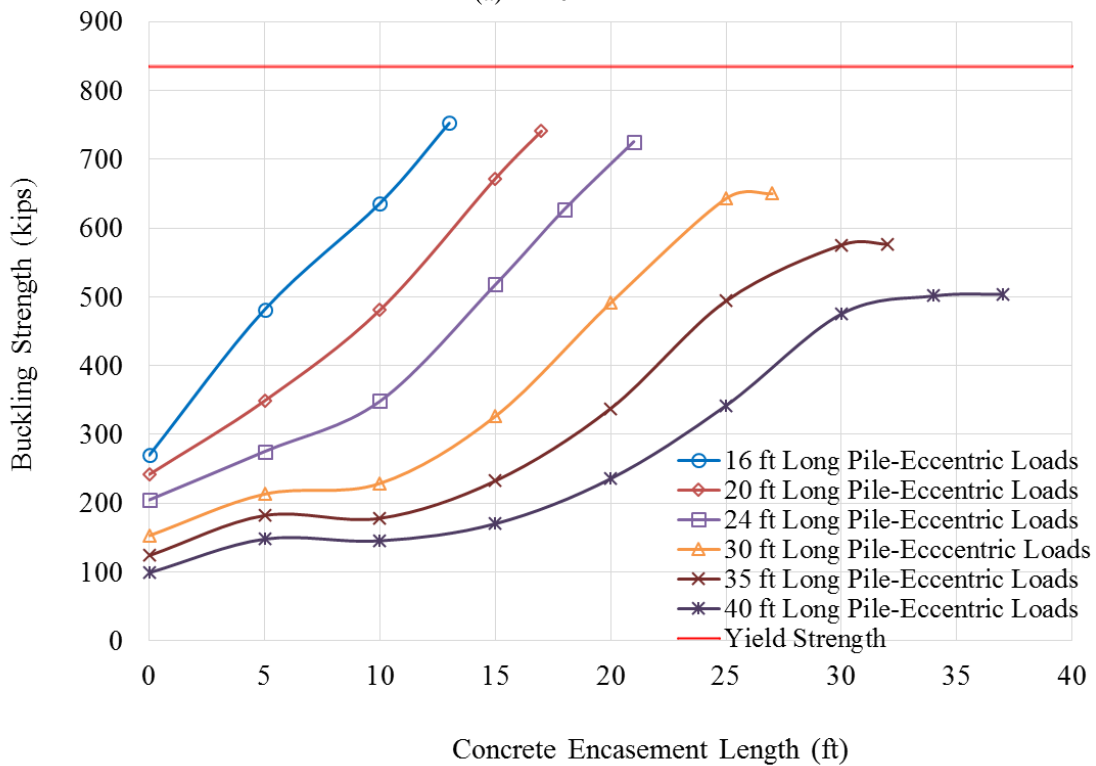


Figure 4.6 Comparisons between the pile strengths derived from the AISC equations and FE results – eccentric loads/no concrete encasement

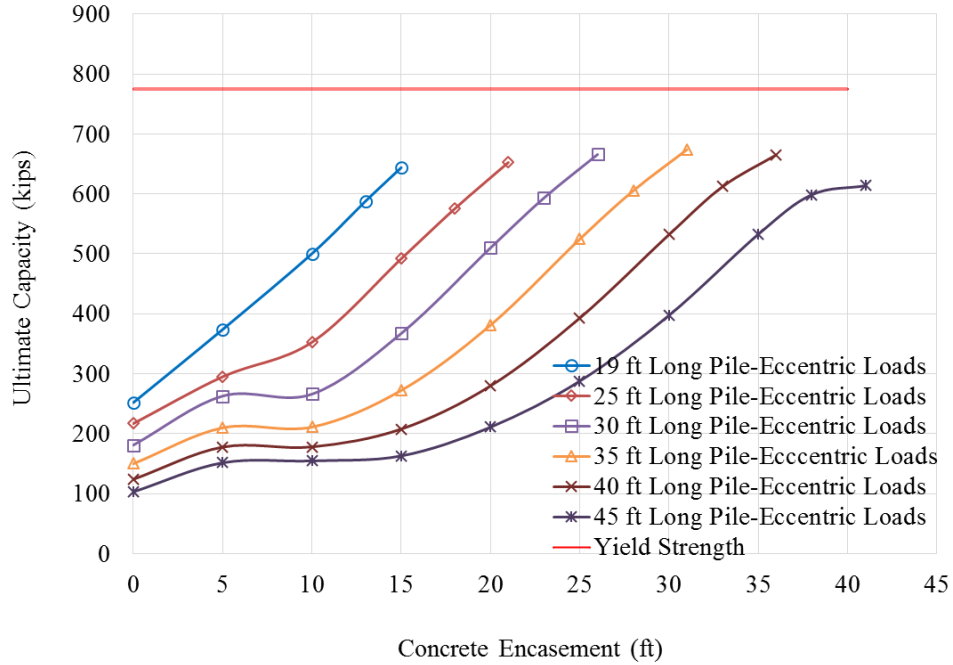
To develop a pile assessment tool, the buckling strength of steel H-piles with eccentric loads/concrete encasement should be calibrated to achieve the same safety margin as steel H-piles with eccentric loads/no concrete encasement, which was also discussed in section 4.3. Therefore, the estimation difference in Table 4.12 though Table 4.21 was deducted from the buckling strength of steel H-piles with eccentric loads/concrete encasement. The calibrated buckling strength of steel H-piles with different concrete encasement lengths under eccentric loads was shown in Figure 4.7.



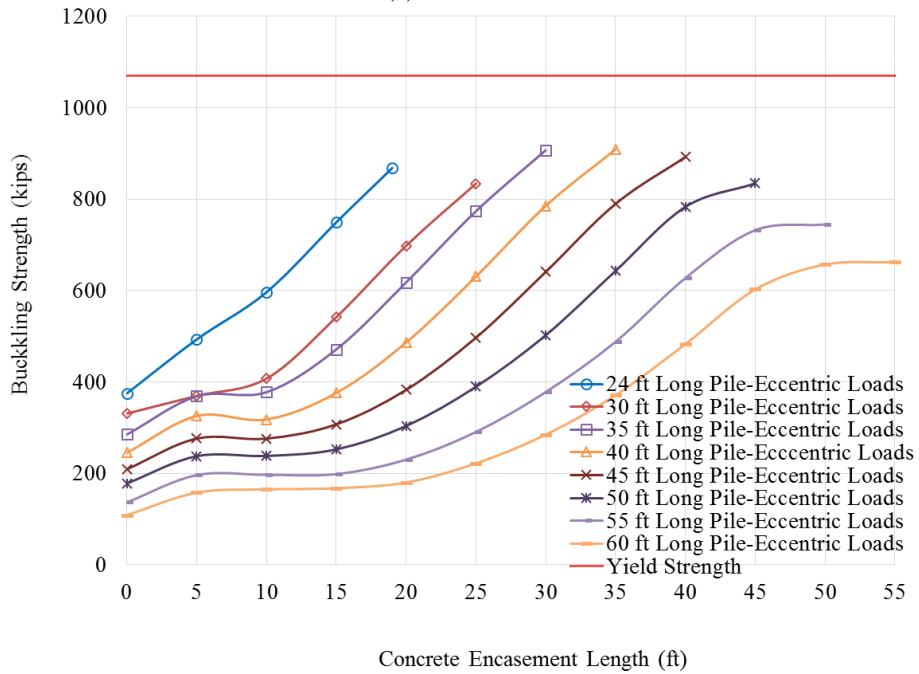
(a) HP10x42



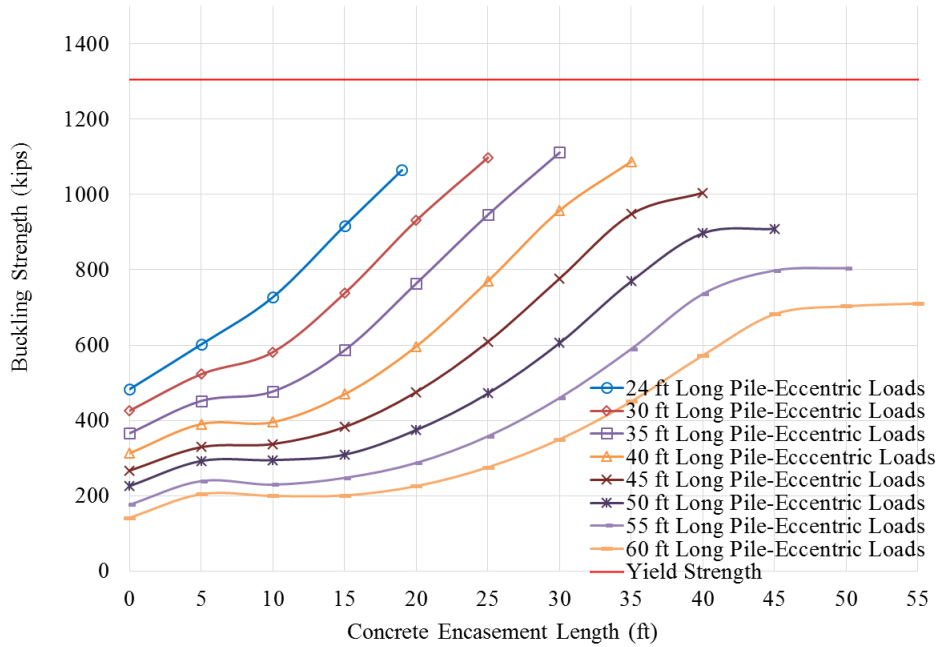
(b) HP10x57



(c) HP12×53



(d) HP14×73



(e) HP14×89

Figure 4.7 Calibrated buckling strength of steel H-piles with different concrete encasement lengths under eccentric loads

Based on the FE results and calibrated results, the buckling strength of steel H-piles with different concrete encasement lengths under concentric and eccentric loads can be directly read from Figure 4.3 and Figure 4.7, respectively. For the unbraced pile lengths not exactly the same as the ones incorporated in Figure 4.3 and Figure 4.7, but within the range of pile lengths used in the FE simulations, appropriate bi-directional linear interpolations should be employed based on the curves shown in Figure 4.3 and Figure 4.7.

Additionally, as part of the goal of this study, a tool was developed to quickly evaluate the buckling strength of steel H-piles with concrete encasement. The curves in Figure 4.3 and Figure 4.7 and appropriate interpolations for every increment of 1-ft pile length were incorporated in the programming. To ensure conservative estimation, if unbraced pile length is not an integer, the length is automatically rounded to the next higher integer in the vicinity of the number by the program. The graphical user interface of the pile assessment tool is shown in Figure 4.8.

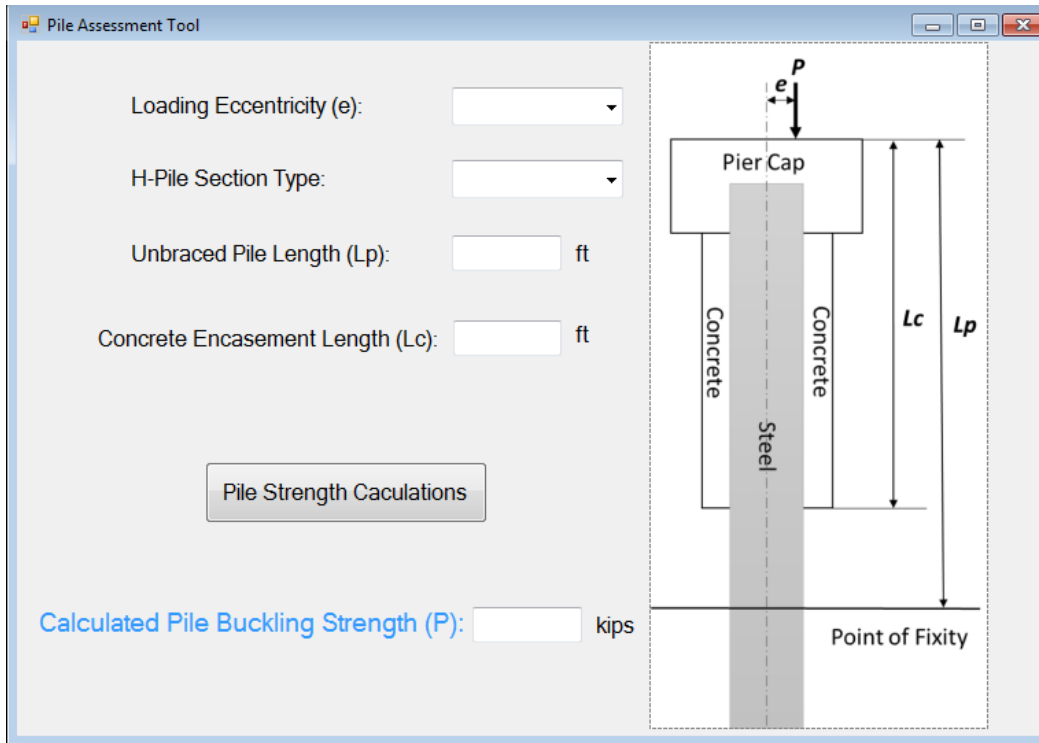


Figure 4.8 Graphical user interface of the pile assessment tool

As shown in Figure 4.8, four parameters must be input in the graphical user interface, i.e., loading eccentricity (e), H-pile section type (HP10×42, HP10×57, HP12×53, HP14×73, or HP14×89), unbraced pile length (L_p), and concrete encasement length (L_c). Once the four parameters have been input, click on the “Pile Strength Calculations” button, and the calculated pile buckling strength (P) will be determined.

CHAPTER 5: SUMMARY AND CONCLUSIONS

Because of the threat posed by scour, the performance of steel piles with partial-length concrete encasements (i.e., step columns) should be evaluated carefully. In this project, a numerical evaluation program was designed and implemented to evaluate steel H-piles with concrete encasements. The numerical program consists of various types of FE models generated using appropriate FE modeling techniques. To validate the FE modeling techniques, FE models were established for steel H-piles without concrete encasements and for steel H-piles with concrete encasements. The FE models were modified to consider both linear elastic buckling analysis and non-linear elastic buckling analysis for the two types of steel H-piles. The load eccentricities were also taken into account in the validated FE models. It is worth noting that geometric imperfection (out-of-straightness) and residual stress were included in the nonlinear FE models, which is consistent with the specifications in the AISC Steel Construction Manual. These FE models were validated against the results derived based on the AISC Steel Construction Manual.

After the FE modeling techniques had been validated, parametric studies were performed to understand the influence of concrete encasements on pile buckling strength. The individually encased pile bents in the P10L standard, which is the current Iowa design standard for pile bents with steel H-piles, were utilized for the parametric studies. Five H-pile sections (HP10×42, HP10×57, HP12×53, HP14×73, and HP14×89) were utilized for the parametric studies. The parameter studies were designed taking into account different combinations of the unbraced pile length and concrete encasement length. The buckling strength of the steel H-piles with concrete encasements was evaluated under two different loading conditions (concentric and eccentric loading conditions). Based on the results from the parametric studies, the relationships of the buckling strength of the steel H-piles with the concrete encasement length were plotted for the five cross-sections and two loading conditions. Since the buckling strength of the steel H-piles without concrete encasement under eccentric loads was conservatively estimated by the AISC Steel Construction Manual, the buckling strength of the steel H-piles with concrete encasements under eccentric loads derived from FE results was calibrated to achieve safety margins similar to those with the AISC manual.

The stiffness contribution of concrete encasements is not taken into account by the AISC Steel Construction Manual (AISC 2017) or the AASHTO LRFD specifications (AASHTO 2015) for estimating the buckling strength of steel H-piles with concrete encasements. A pile assessment tool was developed to quickly calculate the buckling strength of steel H-piles with concrete encasements based on the analysis results. The tool includes the nonlinear relationships between capacity and embedment length for the five cross-sections and two loading conditions. For the user's convenience, a graphical user interface for the pile assessment tool was developed to quickly estimate pile buckling strength. The user must input four parameters: loading eccentricity (e), H-pile section type (HP10×42, HP10×57, HP12×53, HP14×73, or HP14×89), unbraced pile length (L_p), and concrete encasement length (L_c). The pile assessment tool developed through this project can be employed to quickly calculate pile capacity and to assist state rating engineers in making rapid decisions on pile capacity and stability.

REFERENCES

- AASHTO. 2012. *LRFD Bridge Design Specifications, Customary U.S. Units*, 6th Edition. American Association of State Highway and Transportation Officials, Washington, DC.
- . 2015. *LRFD Bridge Design Specifications, Customary U.S. Units*, 7th Edition, with 2015 and 2016 Interim Revisions. American Association of State Highway and Transportation Officials, Washington, DC.
- Abambres, M., and W. M. Quach. 2016. Residual Stresses in Steel Members: A Review of Available Analytical Expressions. *International Journal of Structural Integrity*, Vol. 7, No. 1, pp. 70–94.
- Alpsten, G. 1968. *Thermal Residual Stresses in Hot-Rolled Steel Members*. Paper 329. Fritz Engineering Laboratory, Lehigh University, Lehigh, PA.
- AISC. 1986. *Highway Structures Design Handbook, Volume I*. American Institute of Steel Construction, Chicago, IL.
- . 2017. *AISC Steel Construction Manual*, 15th Edition. American Institute of Steel Construction, Chicago, IL.
- Anderson, J. P. and J. H. Woodward. 1972. Calculation of Effective Lengths and Effective Slenderness Ratios of Stepped Columns. *Engineering Journal*, Vol. 9, pp. 157–166.
- ANSYS. 2012. Release Notes, 14.5 documentation for ANSYS. ANSYS, Inc., Canonsburg, PA. https://www.sharcnet.ca/Software/Ansys/15.0.7/en-us/help/ai_rn_0410.pdf
- Beedle, L.S. and L. Tall. 1960. Basic column strength. *Journal of the Structural Division*, Vol. 86, No. 7, pp. 139–173.
- BSK 99. 2003. Swedish design regulations for steel structures, Boverket, Karlskrona, Sweden.
- Deng, Y. and G. Morcouc. 2013. Efficient Prestressed Concrete-Steel Composite Girder for Medium-Span Bridges: II – Finite Element Analysis and Experimental Investigation. *Journal of Bridge Engineering*, Vol. 18, No. 12, pp. 1358–1372.
- Deng, Y., T. R. Norton, and C. Y. Tuan. 2013. Numerical Analysis of Concrete-Filled Circular Steel Tubes. *Structures and Buildings*, Vol. 166, No. 1, pp. 3–14.
- Deng, Y., B. Phares, A. J. Putz, C. Carter, M. Nop, and D. Bierwagen. 2016a. Performance Evaluation of Longitudinal UHPC Closure Pour Connection for Use in Modular Bridge Construction – A Pairwise Comparison of Capacity and Ductility at Failure Limit State. *Transportation Research Record: Journal of the Transportation Research Board*, No. 2592, pp. 65–75.
- Deng, Y., B. Phares, H. Dang, and J. Dahlberg. 2016b. Impact of Concrete Deck Removal on Horizontal Shear Capacity of Shear Connections. *Journal of Bridge Engineering*, Vol. 21, No. 3, pp. 04015059-1–10
- Deng, Y., B. Phares, and O. W. Steffens. 2016c. Experimental and Numerical Evaluation of a Folded Plate Girder System for Short-Span Bridges – A Case Study. *Engineering Structures*, Vol. 113, pp. 26–40.
- Ellobody, E., B. Young, and D. Lam. 2011. Eccentrically Loaded Concrete Encased Steel Composite Columns. *Thin-Walled Structures*, Vol. 49, No. 1, pp. 53–65.
- European Convention for Constructional Steelwork (ECCS). 1984. *Ultimate Limit State Calculation of Sway Frames with Rigid Joints*. Technical Committee 8 – Structural Stability Technical Working Group 8.2, Issue No. 33, Brussels, Belgium.

- Galambos, T. V. and R. L. Ketter. 1958. Columns Under Combined Bending and Thrust. *Welded Continuous Frames and Their Components*. Progress Report No. 26. Fritz Engineering Laboratory, Lehigh University, Bethlehem, PA.
- Hognestad, E. 1951. *A Study of Combined Bending and Axial Load in Reinforced Concrete Members*. Bulletin No. 399, University of Illinois Engineering Experiment Station, Urbana-Champaign, IL.
- Huber, A. W. 1956. The Influence of Residual Stress on the Instability of Columns. PhD dissertation. Paper 1496. Fritz Engineering Laboratory, Lehigh University, Lehigh, PA.
- Iowa DOT. 2014. Pile Bents with Steel H-Piles, *LRFD Bridge Design Manual Commentary*, CATD 6.6, Office of Bridges and Structures, Iowa Department of Transportation, Ames, IA.
- Kattell, J. and M. Eriksson. 1998. *Bridge Scour Evaluation: Screening, Analysis, & Countermeasures*. United States Department of Agriculture Forest Service, San Dimas Technology and Development Center, San Dimas, CA.
- Lagasse, P. F., P. E. Clopper, L. W. Zevenbergen, and L. W. Girard. 2007. *NCHRP Report 593: Countermeasures to Protect Bridge Piers from Scour*. National Cooperative Highway Research Program, Washington, DC.
- Salmon, C. G. and J. E. Johnson. 1996. *Steel Structures: Design and Behavior: Emphasizing Load and Resistance Factor Design*. HarperCollins, New York, NY.
- Swaminathan, D. and B. Phares. 2015. *Investigation of P10L Piles*. Bridge Engineering Center, Iowa State University, Ames, IA.
- Young, B. W. 1972. Residual Stresses in Hot-Rolled Members, IABSE Int. Coll. on Column Strength, Vol. 85, Paris, pp. 1–30. www.scribd.com/document/285902004/Residual-stresses-in-hot-rolled-members.
- Wee T. H., M. S. Chin, and M. A. Mansur. 1996. Stress-Strain Relationship of High-Strength Concrete in Compression. *Journal of Materials in Civil Engineering*, Vol. 8, No. 2, pp. 70–76.

**THE INSTITUTE FOR TRANSPORTATION IS THE FOCAL POINT FOR TRANSPORTATION
AT IOWA STATE UNIVERSITY.**

InTrans centers and programs perform transportation research and provide technology transfer services for government agencies and private companies;

InTrans manages its own education program for transportation students and provides K-12 resources; and

InTrans conducts local, regional, and national transportation services and continuing education programs.



**IOWA STATE
UNIVERSITY**

Visit www.InTrans.iastate.edu for color pdfs of this and other research reports.